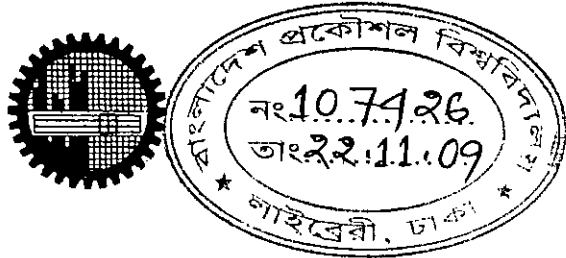


ECG COMPRESSION USING RUN LENGTH ENCODING

by
Shahin Akhter

A Thesis
Submitted to the Department of
Electrical and Electronic Engineering, BUET,
in partial fulfillment of the requirements for the degree of

**MASTER OF SCIENCE IN
ELECTRICAL AND ELECTRONIC ENGINEERING**

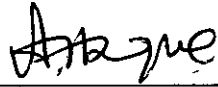





**DEPARTMENT OF ELECTRICAL AND ELECTRONIC ENGINEERING
BANGLADESH UNIVERSITY OF ENGINEERING AND TECHNOLOGY**

November 2009

The thesis titled, “**ECG COMPRESSION USING RUN LENGTH ENCODING**” submitted by **Shahin Akhter**, Roll No: 100506212(P), Session: **October 2005**, has been accepted as satisfactory in partial fulfillment of the requirement for the degree of **Master of Science in Electrical and Electronic Engineering** on **21 November 2009**.

BOARD OF EXAMINERS

1. 
Dr. Md. Aynal Haque
Professor
Dept. of EEE, BUET, Dhaka
Chairman
2. 
Dr. Satya Prasad Majumder
Professor and Head
Dept. of EEE, BUET, Dhaka
Member
(Ex-officio)
3. 
Dr. Newaz Muhammad Syfur Rahim
Associate Professor
Dept. of EEE, BUET, Dhaka
Member
4. 
Dr. Khondkar Siddique-e-Rabbani
Professor and Chairperson
Dept. of Biomedical Physics and Technology
University of Dhaka, Dhaka
Member
(External)

CANDIDATE'S DECLARATION

It is hereby declared that this thesis or any part of it has not been submitted elsewhere for the award of any degree or diploma.

Shahin Akhter

Shahin Akhter

Roll No. 100506212 (P)

Session – October 2005

ACKNOWLEDGEMENTS

The author would like to express his indebtedness and gratitude to his supervisor Dr. Md. Aynal Haque for his endless patience, friendly supervision and invaluable assistance in making a difficult task a pleasant one.

The author wishes to express his thanks and regards to the Head of the Department of Electrical and Electronic Engineering, BUET, Dhaka, for his support during the work.

Sincerest thanks to friends and colleagues for their constant support and criticism of the thesis work.

CONTENTS

Acknowledgements	iv
Abstract	vii
List of Figures	viii
List of Tables	x
CHAPTER 1 INTRODUCTION	1
1.1 Historical Background	1
1.2 Objective of the Thesis	3
1.3 Organization of the Dissertation	4
CHAPTER 2 THE HEART AND THE ECG	5
2.1 Anatomy and Physiology of Human Heart	5
2.2 Components of the Electrocardiogram	8
2.3 ECG Leads	9
CHAPTER 3 SIGNAL COMPRESSION	12
3.1 Compression and distortion measures	12
3.2 Compression measures	13
3.3 Error criterion and distortion measures	13
3.3.1 Percentage root-mean-square difference (PRD)	14
3.3.2 Root mean square (RMS) error	14
3.3.3 WDD index	14
CHAPTER 4 DISCRETE COSINE TRANSFORM (DCT)	17
4.1 Fourier series and Fourier Transform	17
4.2 DCT	19
4.3 Quantization	22
CHAPTER 5 PREPROCESSING OF ECG SIGNAL	24
5.1 QRS detection	25
5.2 T wave detection	30
5.3 P wave detection	32
5.4 Baseline estimation	34
5.5 ST segment features	35
CHAPTER 6 PROPOSED ALGORITHMS AND RESULTS	38
6.1 Proposed Algorithm	38
6.1.1 ECG segmentation	39
6.1.2 DCT Transform	40
6.1.3 Quantization	41
6.1.4 Run length encoding	41
6.1.5 Huffman encoding	42
6.1.6 Bit rate calculation	44

6.2 Test dataset	45
6.3 The values of WDD parameters	45
6.4 Results	47
6.4.1 Comparison with other methods	50
6.4.2 Neural Network based compression	54
CHAPTER 7 CONCLUSION	58
7.1 Discussion	58
7.2 Future Perspectives	59
APPENDIX	60
REFERENCES	61

ABSTRACT

The electrocardiogram (ECG) is one of the most vital medical signals that are recorded for various analysis and diagnostic purposes. Modern clinical systems require effective and economic data storage for telemedicine applications, like telecardiology, to overcome the bandwidth limitations of data transmission channels. Recent advancements in ECG compression reveal that transformational approaches performs better than direct time domain approaches for high compression ratio (CR) and low noise insensitivity. Among the transformational approaches, discrete cosine transform (DCT) is more applicable than others, as it has the energy conservation property that measures the efficiency of the compression scheme directly by tracking its ability to pack input data into as few coefficients as possible.

In this work, we have performed DCT on the time domain ECG signals to obtain the spectral density in spatial domain. Energy compaction property of DCT facilitates the application of quantization by accumulating the correlative coefficients into separate segments. Thus the high probability of redundancies in consecutive coefficients facilitates the use of run length encoding (RLE). Also, less calculation complexity in encoder and decoder makes RLE faster and easier to implement. To increase the CR, two stages of RLE to quantized DCT coefficients are performed. Then Huffman coding is applied on the RLE values to convert them into binary. Here, the preservation of relevant clinical diagnostic information in the reconstructed signal is ensured by measuring the amount of distortion in terms of weighted diagnostic distortion (WDD), percentage root-mean-squared difference (PRD) and root-mean-square (RMS) error indices. The proposed compression algorithm has obtained compression ratio of 14.87 with a bit rate of 185 bps for MIT-BIH Arrhythmia database Record 117.

To compare the performance of the proposed RLE based compression scheme, a 3-layer neural network system is also applied here. Our proposed scheme has shown better CR over neural network based system in terms of WDD, PRD and RMS indices.

List of Figures

2.1	Anatomy of the heart	6
2.2	Components of the ECG	9
2.3	The standard (bipolar) limb leads I, II, and III	10
2.4	The augmented (unipolar) leads aVR, aVL, and aVF	11
2.5	Precordial (unipolar) leads	11
3.1	Some of the diagnostic features of ECG	15
4.1	One dimensional cosine basis function	20
4.2	Graphs of simple quantizer functions	22
5.1	PQRST complexes location points of one beat	25
5.2	Simplified block diagram of the QRS detector	25
5.3	The QRS complex coarse limits estimation process	27
5.4	The estimation process of peaks and exact limits of one QRS complex	29
5.5	Simplified block diagram of the T wave detector	30
5.6	T wave detection	31
5.7	The block diagram of the P wave detector	32
5.8	P wave detection	33
5.9	The flow chart of the primary P shape classification	34
5.10	The flow chart of the P shape decision correction	35
5.11	ECG signal with baseline drift (the dashed line is the estimated baseline)	36
5.12	Baseline Estimation of ECG signal	36
5.13	The ST segment features	37
6.1	Block diagram of our proposed compression scheme	39
6.2	Inter- and intra-beat correlation one beat ECG signal	39
6.3	P, QRS and T features of ECG signal	40
6.4	An example of our RLE based encoding scheme	42
6.5	An Example of Huffman Tree formulation from a given dataset	43
6.6	Original and reconstructed ECG signal after DCT-RLE of record 117 (MIT-BIH)	48

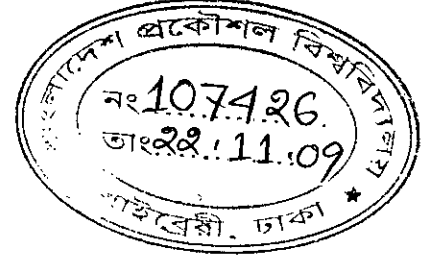
6.7	The compression ratio and distortion-rate curves of our proposed compression scheme for MIT-BIH record 117 with respect to bit rate variation	49
6.8	Original and reconstructed ECG signal after DCT-RLE of record 119 (MIT-BIH)	50
6.9	The compression ratio and distortion-rate curves of our proposed compression scheme for MIT-BIH record 119 with respect to bit rate variation	51
6.10	Original and reconstructed ECG signal after DCT-RLE of record 101 (MIT-BIH)	52
6.11	The distortion-rate curves of the algorithms: ASECWDD, LTP, SAPA2, and AZTEC	53
6.12	A 3-Layer Neural Network	55
6.13	MIT-BIH record 101 after NN based compression	56
6.14	The distortion-rate curves of DCT-RLE and NN based schemes for MIT-BIH record 101	57

List of Tables

5.1	P wave shapes	32
6.1	Huffman dictionary	44
6.2	The numbering of the WDD shape features for the penalty matrices	46
6.3	WDD and PRD variation with Quantization resolution and bit rate (bps) for Record-117	47
6.4	WDD and PRD variation with some other techniques from literature	53
6.5	Results of WDD index, PRD and RMS errors of DCT-RLE based and NN based schemes	56

Chapter 1

INTRODUCTION



Electrocardiogram (ECG) is the graphical representation of the electrical activity of human heart. It shows the potential difference between two points on body surface with respect to time. ECG is largely employed as a diagnostic tool in clinical practice in order to assess the cardiac status of the object. The real-time transmission of the ECG like telemedicine, in urgent situations can improve the survival chances of the patient. However, one of the greatest problems involving this kind of telemedicine application is the network bandwidth. ECG exams may generate too much data, which makes it difficult to apply telecardiology in real time. As an example, with the sampling rate of 360 Hz, 11 bit/sample data resolution, a 24 hours record requires about 43MBytes per channel. This requires enormous storage capacity and network bandwidth for transmission. Therefore, efficient coding of the data is required before transmission. The main goal of any ECG data processor is to obtain a minimum information rate, while retaining the relevant diagnostic information in the reconstructed signal. To measure the relevancy between original and reconstructed signal, most of the researchers uses mathematical calculations like percentage root-mean-squared difference (PRD), root-mean-square (RMS) and etc. This sort of representation has very little impact on clinical diagnosis. But, if characteristic parameters like PQRST shapes, features or amplitudes are utilized for the measurement, then the clinical acceptability of the signal will be achieved. An example of this type of measurement is weighted diagnostic distortion (WDD).

1.1 Historical Background

ECG compression techniques are required to reduce (i) storage requirements of hospital databases and ambulatory ECG data, and (ii) the time to transmit data over telephone lines and other narrowband channels [1]. These requirements motivate researchers to look for efficient compression methodologies to reduce the amount of

data. Numerous methods for compressing ECG signal have been proposed and published over the last four decades. Compression methods used for ECG signal can be classified into three major categories [2]:

- 1) Direct time-domain techniques (DTT)
- 2) Transformational approaches (TA)
- 3) Parameter extraction techniques (PET)

DTT methods usually rely on utilizing prediction or interpolation algorithms as amplitude zone-time epoch coding [3] and turning point [4]. In most of the cases, they are superior to TA with respect to the system simplicity and error. However, TA methods usually achieve higher compression ratio (CR), and are insensitive to noise in ECG signals [5]. Some applications of TA methods are wavelet transform [1], [2], [6], discrete cosine transform (DCT) [7], [8] and etc. Here, the original samples are subjected to a linear transformation followed by proper encoding of the transformed output [6], [7]. Some recent one dimensional (1-D) and two dimensional (2-D) wavelet transform based compression schemes with low reconstruction error and smooth signal quality are presented in literature [1], [2], [6]. Although they can achieve high CR, because of the requirements of accurate QRS detection, period normalization, amplitude normalization and mean removal, the 2-D system becomes complex. Again, the complexities of 2-D systems become crucial for real-time transmission, as they introduce delays and these schemes are not suitable for transmission of ECG data through low bandwidth networks. A DCT based scalar quantizer with linear coding has achieved a good CR with excellent reconstruction quality and minimum PRD [7]. Because, DCT transform has the property to provide a large number of small coefficients, which can be zeroed without altering the signal significantly. To facilitate this interesting property of DCT, linear encoding can be performed on the quantized DCT coefficients. As a linear encoder RLE is more acceptable than others as one of the main advantages of RLE is its lower calculation complexity with easier encoding and decoding stages. That makes it fast and easy to implement in comparison with other encoding methods to perform better compression without distortion [2].

Again, up to now, usually researchers utilize simple mathematical distortion measures like percentage PRD, mean squared error (MSE), RMS etc. to evaluate the reconstructed signal quality. Among them, PRD is the most widely used index for evaluation of distortion, because of its simplicity and mathematical convenience [2]. But PRD is not a good measure of the true compression error and results in poor diagnostic relevance [9]. Thus, from the point of view of diagnosis, a standard methodology should be maintained to ensure the acceptability and reliability of the reconstructed ECG data obtained from various compression schemes. Also, due to the dependency on the dc level, PRD can introduce confusion in the evaluation of ECG compressors [10]. Such measures are also irrelevant from the point of view of diagnosis [9]-[11]. So, the use of a distortion measure such as WDD index can be an effective tool for determining the performance of a compression algorithm [11]-[13]. Thus, the utilization of WDD instead of PRD or RMS as distortion measurement technique increases the reliability of the reconstructed ECG signal. Throughout the research work we have tried to utilize the positive impact of WDD on the relevancy of clinical diagnosis, instead of PRD.

1.2 Objective of The Thesis

ECG data compression algorithm leads to a conflicting result which requires a high CR over good signal fidelity. So it is necessary to design a compression scheme which preserves diagnostically important information by offering high compression ratio. Reconstructed signal should have as much low WDD value as possible at high compression ratios.

In this thesis, to compress an ECG signal a DCT based RLE is performed. And also, WDD based distortion index is used to measure the efficiency of the compression scheme. As WDD based distortion index is a less widely used technique in literature, an artificial neural network (ANN) based compression scheme is also developed in this research work to facilitate the performance evaluation process of proposed DCT based scheme. The objectives of this research are:

1. To implement a less complex and faster algorithm with easier coding for ECG signal compression.
2. To ensure that a high CR can be achieved on the point of clinical diagnostic relevancies after reconstruction.
3. To evaluate the performance of the proposed compression scheme using standard database and compare it with a NN based technique using WDD, PRD and RMS error indices.

1.3 Organization of the Dissertation

The thesis begins with an overview of the factors motivating the design of an effective ECG compression scheme that preserves signal information important to disease diagnosis. This overview leads to the formulation of objectives, strategy and scope of thesis. The structure of this work is:

Chapter 1 is a preface and contains the introduction and the purpose of this work.

Chapter 2 describes the physiological background of the heart and the ECG signal.

Chapter 3 presents review of some distortion and compression measures and describes the problem with the standardization of the distortion measures.

Chapter 4 This chapter discusses the concept of DCT-based compression techniques in detailed.

Chapter 5 describes the methods for feature extraction from the ECG signal that are implemented in the pre-processing stage of ECG analysis.

Chapter 6 describes the proposed RLE based ECG compression scheme in detail. It also includes the results of the proposed compression algorithm. Here we have analyzed the performance of our proposed compression scheme by developing an ANN based compression system to perform with the same test conditions. Some existing DCT and RLE based compression techniques are also used for performance comparison.

Chapter 7 contains a summary, conclusions, and recommendations for continuation.

Chapter 2

THE HEART AND THE ECG

Electrocardiograms are signals that originate from the action of the human heart. They are largely employed as a diagnostic tool in clinical practice in order to assess the cardiac status of object like the examination of ambulatory patients or patients in intensive care. Recordings are examined by a physician who visually checks features of the signal and perform estimation of the most important parameters of the signal to provide suggestions accordingly. Proper investigation of the condition of patient may become difficult if there exists variations (size, duration and etc.) in the characteristics parameters of ECG or exists a considerable amount of noise in the signal. So, to highlight the purpose of recognition and analysis of ECG signal in the sense of diagnosis this chapter contains a detailed description of the heart, its activity and the electrocardiogram.

2.1 Anatomy and Physiology of Human Heart

The sole purpose of the heart is to circulate blood through the blood circulatory systems of the body that consists of four hollow chambers (Figure 2.1) [14]. The upper two chambers, the right and left atria, are thin-walled; the lower two, the right and left ventricles are thick-walled and muscular. The walls of the ventricles are composed of three layers of tissue: the innermost thin layer is called the endocardium; the middle thick, muscular layer, the myocardium; and the outermost thin layer, the epicardium. The walls of the left ventricle are more muscular and about three times thicker than those of the right ventricle.

The atrial walls are also composed of three layers of tissue like those of the ventricles, but the middle muscular layer is much thinner. The two atria form the base of the heart; the ventricles form the apex of the heart.

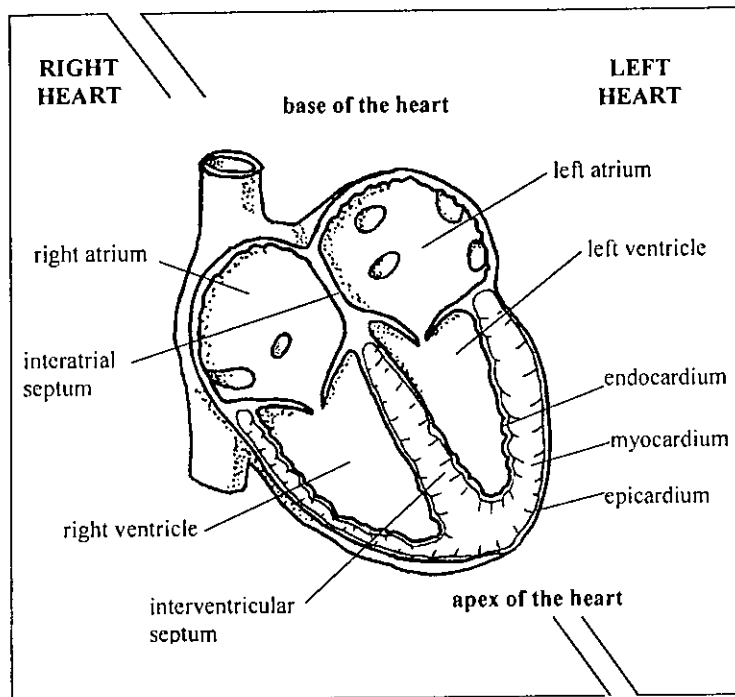


Figure 2.1: Anatomy of the heart

The inter-atrial septum (a thin membranous wall) separates the two atria, and a thicker, more muscular wall, the inter-ventricular septum, separates the two ventricles. The two septa, in effect, divide the heart into two pumping systems, the right heart and the left heart, each one consisting of an atrium and a ventricle.

The right heart pumps blood into the pulmonary circulation (the blood vessels within the lungs and those carrying blood to and from the lungs). The left heart pumps blood into the systemic circulation (the blood vessels in the rest of the body and those carrying blood to and from the body).

The right atrium receives unoxygenated blood from the body via two of the body's largest veins (the superior vena cava and inferior vena cava) and from the heart itself by way of the coronary sinus. The blood is delivered to the right ventricle through the tricuspid valve. The right ventricle then pumps the unoxygenated blood through the pulmonic valve and into the lungs via the pulmonary artery. In the lungs, the blood picks up oxygen and releases excess carbon dioxide.

The left atrium receives the newly oxygenated blood from the lungs via the pulmonary veins and delivers it to the left ventricle through the mitral valve. The left ventricle then pumps the oxygenated blood out through the aortic valve and into the aorta, the largest artery in the body. From the aorta, the blood is distributed throughout the body where the blood releases oxygen to the cells and collects carbon dioxide from them.

The heart performs its pumping action over and over in a rhythmic sequence. First, the atria relax (atrial diastole), allowing the blood to pour in from the body and lungs. As the atria fill with blood, the atrial pressure rises above that in the ventricles, forcing the tricuspid and mitral valves to open and allowing the blood to empty rapidly into the relaxed ventricles. Then the atria contract (atrial systole), filling the ventricles to capacity.

Following the contraction of the atria, the pressures in the atria and ventricles equalize, and the tricuspid and mitral valves begin to close. Then, the ventricles contract vigorously, causing the ventricular pressure to rise sharply. The tricuspid and mitral valves close completely, and the aortic and pulmonic valves snap open, allowing the blood to be ejected forcefully into the pulmonary and systemic circulations.

Meanwhile, the atria are again relaxing and filling with blood. As soon as the ventricles empty of blood and begin to relax, the ventricular pressure falls, the aortic and pulmonic valves shut tightly, the tricuspid and mitral valves open, and the rhythmic cardiac sequence begins anew.

The period from the opening of the aortic and pulmonic valves to their closing, during which the ventricles contract and empty of blood, is called ventricular systole. The following period from the closure of the aortic and pulmonic valves to their reopening, during which the ventricles relax and fill with blood, is called ventricular diastole. The sequence of one ventricular systole followed by a ventricular diastole is

called the cardiac cycle, commonly defined as the period from the beginning of one heart beat to the beginning of the next.

2.2 Components of the Electrocardiogram

The impulse as it crosses the heart can be observed by measuring the electrical current with electrodes placed on the patient's skin in relative and specific places. This impulse, when filtered through a specially designed machine called electrocardiogram, produces characteristic waveforms that can be compared to established normal waveforms and some other information about the current state of the heart is determined. The electric current generated by atrial depolarization is recorded as the P wave, and that generated by ventricular depolarization is recorded as the Q, R, and S waves: the QRS complex. Atrial repolarization is recorded as the atrial T wave (Ta), and ventricular repolarization, as the ventricular T wave, or simply, the T wave. Because atrial repolarization normally occurs during ventricular depolarization, the atrial T wave is buried or hidden in the QRS complex.

In a normal cardiac cycle, the P wave occurs first, followed by the QRS complex and the T wave (Figure 2.2) [13].

The sections of the ECG between the waves and complexes are called segments and intervals: the PR segment, the ST segment, the TP segment, the PR interval, the QT interval, and the R-R interval. Intervals include waves and complexes, whereas segments do not. The normal ECG complex consists of three key elements, in parenthesis is presented the amplitude:

- the P-Wave, representing the impulse across the atria to the AV node (0.25 mV)
- the QRS representing the impulse as it travels across the ventricles (R-1.6 mV, Q, S-25% of R wave)
- the T-Wave, representing the repolarization of the ventricles (0.1-0.5 mV)

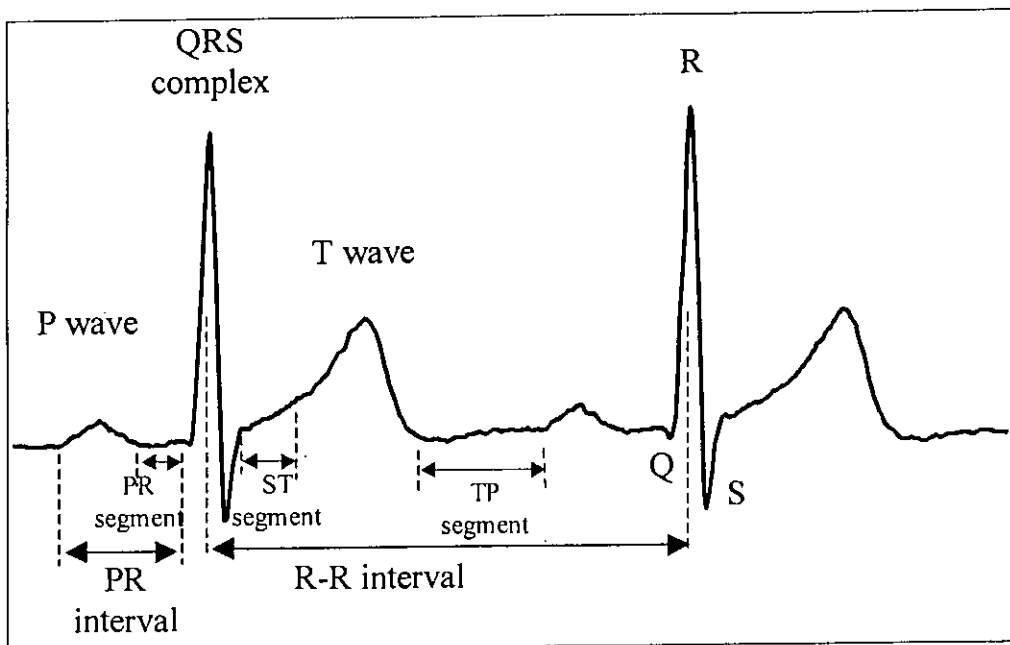


Figure 2.2: Components of the ECG

When electrical activity of the heart is not being detected, the ECG is a straight, flat line as like as the isoelectric line or baseline.

2.3 ECG Leads

An ECG lead is a record (spatial sampling) of the electrical activity generated by the heart that is sensed by either one of two ways: (1) two discrete electrodes of opposite polarity or (2) one discrete positive electrode and an “indifferent,” zero reference point. A lead composed of two discrete electrodes of opposite polarity is called a bipolar lead; a lead composed of a single discrete positive electrode and a zero reference point is a unipolar lead.

Depending on the ECG lead being recorded, the positive electrode may be attached to the right or left arm, the left leg, or one of several locations on the anterior chest wall. The negative electrode is usually attached to an opposite arm or leg or to a reference point made by connecting the limb electrodes together.

For a detailed analysis of the heart’s electrical activity, usually in the hospital setting, an ECG recorded from 12 separate leads (the 12-lead ECG) is used. The 12-lead

ECG is also used in the pre-hospital phase of emergency care in certain advanced life support services to diagnose acute myocardial infarction and to help in the identification of certain arrhythmias. A 12-lead ECG consists of three standard (bipolar) limb leads (leads I, II, and III) (Figure 2.3), Three augmented (unipolar) leads (leads aVR, aVL, and aVF) (Figure 2.4), and six precordial (unipolar) leads (V₁, V₂, V₃, V₄, V₅, and V₆) (Figure 2.5) [13]. When monitoring the heart solely for arrhythmias, a single ECG lead, such as the standard limb lead II, is commonly used, especially in the pre-hospital phase of emergency care.

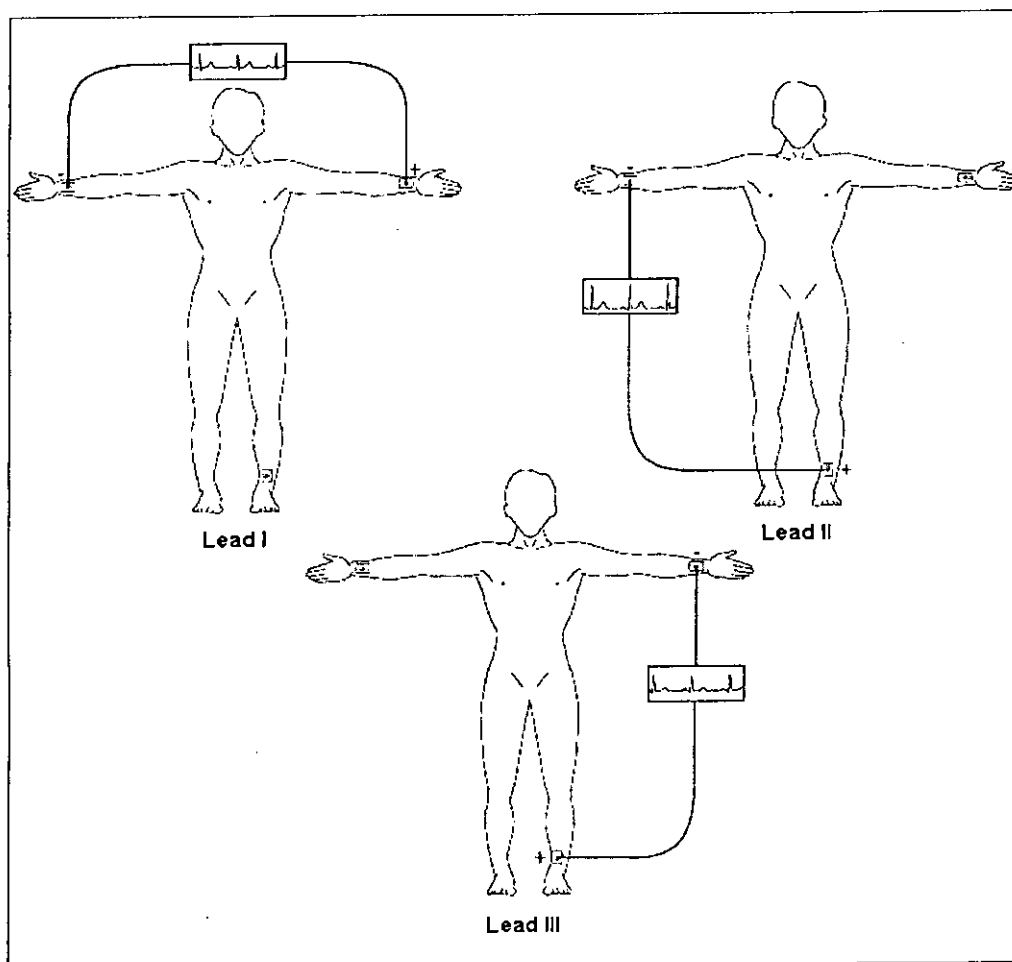


Figure 2.3: The standard (bipolar) limb leads I, II, and III

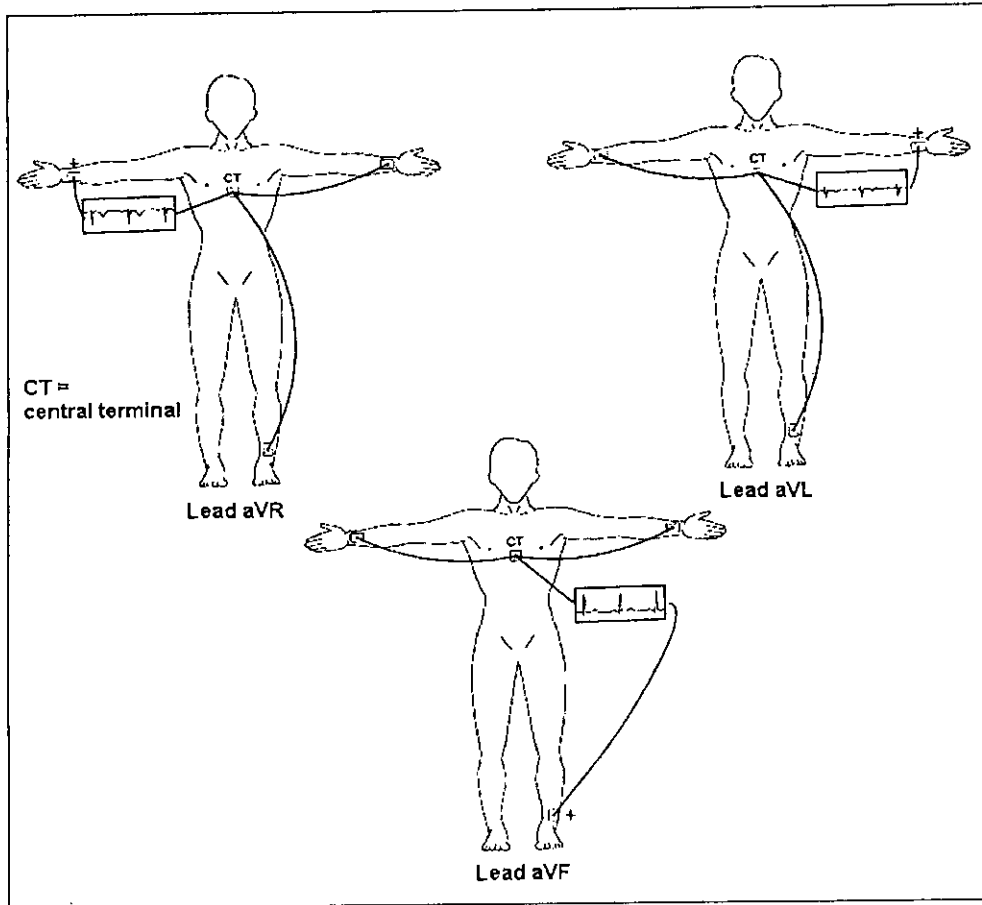


Figure 2.4: The augmented (unipolar) leads aVR, aVL, and aVF

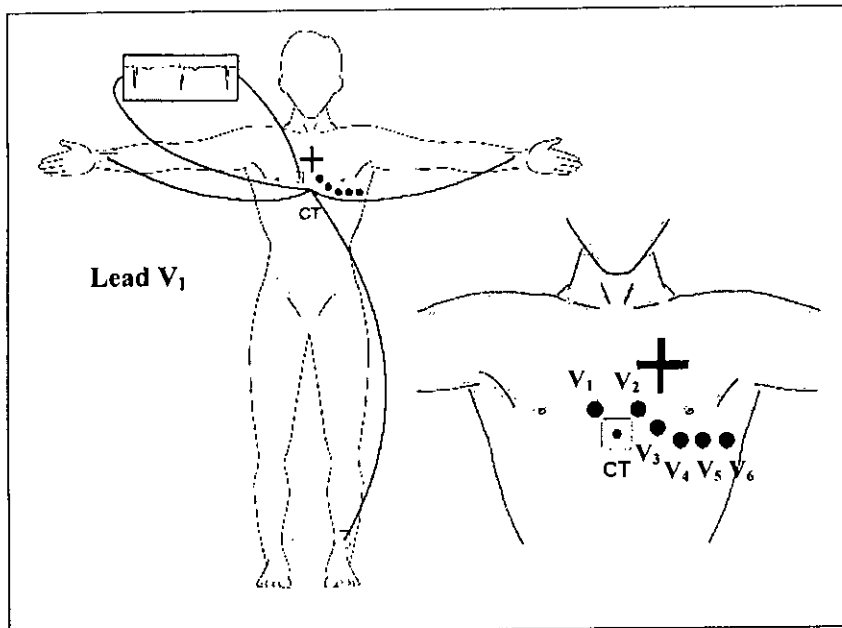


Figure 2.5: Precordial (unipolar) leads

Chapter 3

SIGNAL COMPRESSION

A typical computerized medical signal processing systems requires a large amount of data to examine the condition of the patient, which is difficult to store and transmit [16]. So, it is very desirable to find a method of reducing the quantity of data without a little or no loss of important information. A solution to this problem is the application of data compression that tries to obtain a minimum data storage by eliminating redundancy where possible. The compression performance is measured as the ratio of the number of bits of the original signal to the number stored in the compressed signal. A high CR is wanted, typically, but using this alone to compare data compression algorithms is not acceptable. Generally the bandwidth, sampling frequency, and precision of the original data very much affect the CR [5].

A data compression algorithm must also retrieve the data with acceptable fidelity. In biomedical data compression, the clinical acceptability of the reconstructed signal has to be determined through visual inspection. The residual between the reconstructed signal and the original signal may also be measured by numerical methods. Here a lossless data compression algorithm produces zero residual, and the reconstructed signal exactly replicates the original signal. However, clinically acceptable quality is neither guaranteed by a low nonzero residual nor ruled out by a high numerical residual [10], [17]. This chapter focuses on the definitions of various terminologies that are commonly used in the field of data compression.

3.1 Compression and distortion measures

The criterion for testing performance of compression algorithms includes three components: compression measure, reconstruction error and computational complexity. The compression measure and the reconstruction error are usually dependent on each other and are used to create the rate-distortion function of the

algorithm. The computational complexity component is part of the practical implementation consideration but it is not part of any theoretical measure.

3.2 Compression measures

The size of compression is often measured by the CR which is defined as the ratio between the bit rate of the original signal and the bit rate of the reconstructed one:

$$CR = \frac{b_{orig.}}{b_{comp.}} \quad (3.1)$$

Here problem arises from the application of different sampling frequencies and different number of quantization levels; thus, the bit rate of the original signal is not standard. Use of the number of bits transmitted per sample of the compressed signal as a measure of information rate removes the dependency on the quantizer resolution, but the dependence on the sampling frequency remains. Another way to remove the dependency on quantizer's resolution and sampling frequency is the use of bits transmitted per second.

3.3 Error criterion and distortion measure

One of the most difficult problems in ECG compression applications and reconstruction is defining the error criterion. The purpose of the compression system is to remove redundancy, the irrelevant information (which does not contain diagnostic information – in the ECG case). Consequently the error criterion has to be defined such that it will measure the ability of the reconstructed signal to preserve the relevant information. Such a criterion has been defined in the past as "diagnostability" [18]. Today the accepted way to examine diagnostability is to get cardiologists' evaluations of the system's performance. This solution is good for getting evaluations of coders' performances, but it can not be used as a tool for designing ECG coders and certainly, can not be used as an integral part of the compression algorithm. However, in order to use such a criterion for coders design, one has to give it a mathematical model that represents the deviation of the original and reconstructed signal. An example of this type of model is WDD that compares predefined characteristic features of original and reconstructed ECG signals.

3.3.1 PERCENTAGE ROOT-MEAN-SQUARE DIFFERENCE (PRD)

PRD measure is defined as follows,

$$PRD = \sqrt{\frac{\sum_{n=1}^N ((x(n) - \hat{x}(n)))^2}{\sum_{n=1}^N (x(n) - \bar{x}(n))^2}} \times 100 \quad (3.2)$$

where $x(n)$ is the original signal, $\hat{x}(n)$ is the reconstructed signal, $\bar{x}(n)$ is the mean of the original signal and N is the size of the window over which PRD is calculated.

3.3.2 ROOT MEAN SQUARE (RMS) ERROR

The RMS is defined as

$$RMS = \sqrt{\frac{\sum_{n=1}^N ((x(n) - \hat{x}(n)))^2}{N}} \quad (3.3)$$

where N is the length of the window over which reconstruction is performed.

3.3.3 WDD INDEX

WDD index is based on comparison of the relative preservation of the diagnostic information in PQRST complex features of the original ECG signal and the reconstructed signal. These PQRST complex features are the location, duration, amplitudes, and shapes of the waves that exist in every beat as shown in Figure 3.1. These diagnostic features were chosen with the help of an experienced cardiologist [13].

For every beat of the original signal and for the reconstructed signal, a vector of diagnostic features is defined as in (3.1) and (3.2),

$$\beta^T = [\beta_1, \beta_2, \dots, \beta_p] ; \text{Original signal} \quad (3.4)$$

$$\hat{\beta}^T = [\hat{\beta}_1, \hat{\beta}_2, \dots, \hat{\beta}_p] ; \text{Reconstructed signal} \quad (3.5)$$

where p is the number of features in the vector.

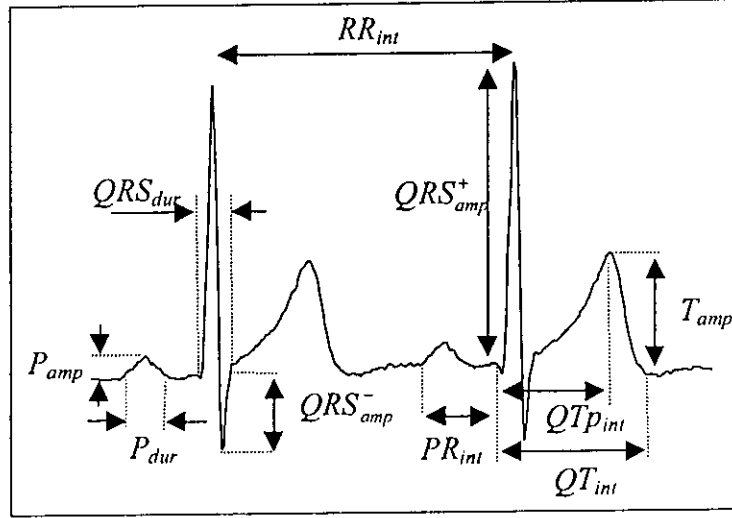


Figure 3.1: Some of the diagnostic features of ECG

The number of features $p = 18$ is used in this work. The diagnostic parameters (β_i , $i = 1, 2, \dots, p$) are chosen as follows: RR_{int} , QRS_{dur} , QT_{int} , QTp_{int} , P_{dur} , PR_{int} , QRS_{peaks_no} (the number of peaks and notches in the QRS complex), Q_{wave_exist} (the sign of the first peak in the QRS), Δ_{wave_exist} (the existence of delta wave), T_{shape} , P_{shape} , ST_{shape} , QRS_{amp}^+ , QRS_{amp}^- , P_{amp} , T_{amp} , $ST_{elevation}$, ST_{slope} as shown in Figure 3.1 [13]:

The WDD index between these two vectors is:

$$WDD(\beta, \hat{\beta}) = \Delta\beta^T \cdot \frac{\hat{\Lambda}}{tr[\hat{\Lambda}]} \cdot \Delta\beta \times 100 \quad (3.6)$$

where $\Delta\beta$ is the normalized difference vector as,

$$\Delta\beta^T = [\Delta\beta_1, \Delta\beta_2, \dots, \Delta\beta_p] \quad (3.7)$$

For the duration features and the amplitude features, the difference is defined as:

$$\Delta\beta_i = \frac{|\beta_i - \hat{\beta}_i|}{\max\{|\beta_i|, |\hat{\beta}_i|\}} \quad (3.8)$$

For the shape features (T_{shape} , P_{shape} , and ST_{shape}) the difference is determined by fixed penalty matrices (one matrix for each shape feature):

$$W^i = \begin{bmatrix} w'_{11} & w'_{12} & \cdot & \cdot & w'_{1z} \\ w'_{21} & w'_{22} & \cdot & \cdot & w'_{2z} \\ \cdot & \cdot & \cdot & \cdot & \cdot \\ \cdot & \cdot & \cdot & \cdot & \cdot \\ w'_{z1} & w'_{z2} & \cdot & \cdot & w'_{zz} \end{bmatrix} \quad (3.9)$$

where Z is the number of shapes for the relevant feature ($Z = 9$ for P_{shape} , $Z = 5$ for ST_{shape} , and $Z = 3$ for T_{shape}). w'_{fg} is the difference between the shape f and the shape g of the original shape feature β_i , and the reconstructed one $\hat{\beta}_i$, respectively. The penalty matrix used here for shape features (P_{shape} , T_{shape} and ST_{shape}) are as follows:

$$W^P = \begin{bmatrix} 0 & .2 & .2 & .2 & .3 & .2 & .2 & .2 & .4 \\ .2 & 0 & .1 & .1 & .3 & .4 & .4 & .4 & .2 \\ .2 & .1 & 0 & .1 & .3 & .4 & .4 & .4 & .2 \\ .2 & .1 & .1 & 0 & .3 & .4 & .4 & .4 & .2 \\ .3 & .3 & .3 & .3 & 0 & .3 & .3 & .3 & .3 \\ .2 & .4 & .4 & .4 & .3 & 0 & .1 & .1 & .2 \\ .2 & .4 & .4 & .4 & .3 & .1 & 0 & .1 & .2 \\ .2 & .4 & .4 & .4 & .3 & .1 & .1 & 0 & .2 \\ .4 & .2 & .2 & .2 & .3 & .2 & .2 & .2 & 0 \end{bmatrix}$$

$$W^T = \begin{bmatrix} 0 & .2 & .4 \\ .2 & 0 & .2 \\ .4 & .2 & 0 \end{bmatrix}$$

$$W^{ST} = \begin{bmatrix} 0 & .1 & .2 & .1 & .4 \\ .1 & 0 & .2 & .4 & .1 \\ .2 & .2 & 0 & .2 & .2 \\ .1 & .4 & .2 & 0 & .1 \\ .4 & .1 & .2 & .1 & 0 \end{bmatrix}$$

Finally, the diagonal weighting matrix can be defined as,

$$\Lambda = \text{diag} [\lambda_i], \lambda_i > 0; i = (1, 2, \dots, p). \quad (3.10)$$

The diagonal weighting matrix used in the present work is as follows,

$$\Lambda = \begin{bmatrix} 2 & 1 & 1 & 1 & 1 & 1 & 1 & 0.25 & 0.25 & 1 & 1 & 2 & 2 & 1 & 1 & 1 & 1 \end{bmatrix}$$

Chapter 4

DISCRETE COSINE TRANSFORM (DCT)

Transform-based ECG compression methods use an invertible orthogonal transformation to the signal that helps to reduce the redundancy present in the new representation. A transformation is, therefore, defined to map this spatial (correlated time domain) data into transformed (Uncorrelated) coefficients. Due to the decorrelation and energy compaction properties, transform domain approaches like cosine [7], [8], [19], and wavelet [1], [2], [6], [20] transforms are widely investigated for data compression. For example DCT has been used for ECG compression [7], [8], [21]–[23]. As transformation is a lossless operation, therefore, the inverse transformation produces a perfect reconstruction of the original data. This chapter contains detail discussion on the origin of DCT and also its application in the field of data compression.

4.1 Fourier series and Fourier Transform

Frequency representation of periodic functions in terms of series of sines and cosines is known as Fourier series. So, for a periodic signal $f(t)$, Fourier series will be,

$$f(t) = a_0 + \sum_{n=1}^{\infty} a_n \cos nw_0t + \sum_{n=1}^{\infty} b_n \sin nw_0t, \quad (4.1)$$

where $w_0 = \frac{2\pi}{T}$.

The Equation (4.1) can be written as:

$$f(t) = \sum_{n=-\infty}^{\infty} c_n e^{jnw_0t}$$

The concept of Fourier series can be extended through some modifications to obtain the representation for non periodic signals. The equation for Fourier transform and its inverse is shown in Equation (4.2) and (4.3) respectively.

$$F(\omega) = \int_{-\infty}^{\infty} f(t)e^{-j\omega t} dt \quad (4.2)$$

$$f(t) = \frac{1}{2\pi} \int_{-\infty}^{\infty} F(\omega)e^{j\omega t} d\omega \quad (4.3)$$

The function $F(\omega)$ can represent the fluctuations of the signal at different frequencies. And the inverse of the transform shows the ability to accumulate the fluctuating components at different frequencies. The reversible process of Fourier transform ensures that the process is energy-preserving. The property reveals that the total energy content remains same both in time and frequency domains. This can be shown by Equation (4.4).

$$\int_{-\infty}^{\infty} |f(t)|^2 dt = \frac{1}{2\pi} \int_{-\infty}^{\infty} |F(\omega)|^2 d\omega, \quad (4.4)$$

where, $\omega = 2\pi f$.

The procedures of Fourier series and transform are based on signals that are continuous function of time. But in practical situations, most of the signals are the samples of continuous signal at different moments. To deal with this type of signals, Discrete Fourier transform (DFT) is introduced from Fourier series. The Fourier series coefficient c_k of continuous function $f(t)$ is changed to a repetitive function of N samples within a time interval T .

Periodic representation of coefficients c_k in Equation (4.5) has been changed to Equation (4.6).

$$c_k = \frac{1}{T} \int_0^T f(t)e^{jk\omega_0 t} dt \quad (4.5)$$

$$F_k = \frac{1}{T} \int_0^T f(t) \sum_{n=0}^{N-1} \delta(t - \frac{n}{N}T) e^{jk\omega_0 t} dt \quad (4.6)$$

where, $\omega_0 = \frac{2\pi}{T}$.

The only difference between the representations is the duration where one is the period of the other periodic sequence. But the main drawback of this assumption of a non periodic signal to a periodic sequence using DFT is that there introduces a sharp discontinuity at the beginning and end of DFT sequences. In order to represent the sharp discontinuity, DFT needs to keep its higher frequency components as nonzero. Normally, transform based data compression schemes eliminates the high frequency components of the transformed coefficients. But, as the high frequency content is a necessity for DFT, the coefficient reduction introduces distortions in the retrieved data sequences. So, if there could be introduced a mirroring effect of DFT coefficients by doubling the period N , the effect of sharp discontinuity at the edges can be eliminated.

An example of this type of application is the DCT that is the first N -points of the resulting $2N$ -point DFT. This DCT should have more energy-compaction property than DFT as the effect of high frequency components can now be neglected easily. So in terms of CR, the DCT performs better than DFT.

4.2 DCT

The most common DCT definition of a 1-D sequence of length N is

$$C(u) = \alpha(u) \sum_{x=0}^{N-1} f(x) \cos\left[\frac{\pi(2x+1)u}{2N}\right] \quad (4.7)$$

For $u = 0, 1, 2, \dots, N-1$.

Similarly, the inverse transformation is defined as

$$f(x) = \sum_{u=0}^{N-1} \alpha(u) C(u) \cos\left[\frac{\pi(2x+1)u}{2N}\right] \quad (4.8)$$

For $x = 0, 1, 2, \dots, N-1$.

In both equations (4.7) and (4.8) $\alpha(u)$ is defined as,

$$\alpha(u) = \begin{cases} \sqrt{\frac{1}{N}} & \text{For } u = 0 \\ \sqrt{\frac{2}{N}} & \text{For } u \neq 0 \end{cases} \quad (4.9)$$

It is clear from Figure 4.1, that the first transform coefficient is the average value of the sample sequence. In literature of DCT, this value is referred to as the *DC Coefficient*. All other transform coefficients are called the *AC Coefficients*.

To visualize the ideas of DCT, variations of u is plotted in Figure 4.1 for $N = 8$ by ignoring $f(x)$ and $\alpha(u)$ as follows:

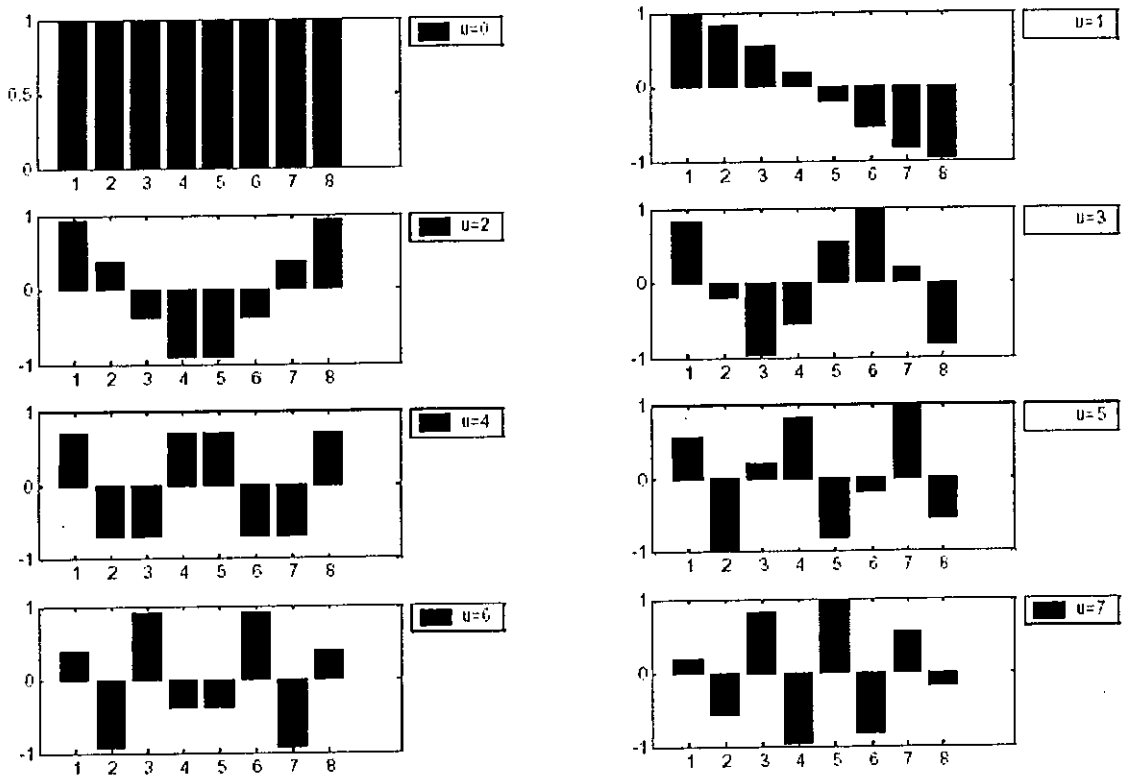


Figure 4.1: One dimensional cosine basis function ($N=8$)

From previous discussions on 1-D DCT, the first the top-left waveform in Figure 4.1 shows a constant (DC) value, whereas, all other waveforms ($u = 1, 2 \dots 7$) shows a progressive increase of frequencies [19]. These waveforms are called the *cosine basis function*. They are the orthogonal basis function of DCT. Because, multiplication of any waveform in Figure 4.1 with another waveform followed by a summation over all sample points yields a zero (scalar) value, whereas multiplication

of any waveform in Figure 4.1 with itself followed by a summation yields a constant (scalar) value. Also, orthogonal waveforms are always independent as none of the basis functions can be represented as a combination of other basis functions [19].

The 1-D DCT can be directly extended to the 2-D DCT as is given in Equation (4.10).

$$C(u, v) = \alpha(u)\alpha(v) \sum_{x=0}^{N-1} \sum_{y=0}^{N-1} f(x, y) \cos\left[\frac{\pi(2x+1)u}{2N}\right] \cos\left[\frac{\pi(2y+1)v}{2N}\right] \quad (4.10)$$

For $u, v = 0, 1, 2, \dots, N-1$.

The inverse transform is:

$$f(x, y) = \sum_{u=0}^{N-1} \sum_{v=0}^{N-1} \alpha(u)\alpha(v)C(u, v) \cos\left[\frac{\pi(2x+1)u}{2N}\right] \cos\left[\frac{\pi(2y+1)v}{2N}\right] \quad (4.11)$$

For $x = 0, 1, 2, \dots, N-1$.

Basis functions for the 2-D can be generated by multiplying the horizontally oriented 1-D basis functions (shown in Figure 4.1) with vertically oriented set of the same functions. Here a progressive increase of frequencies occur both in the vertical and horizontal directions.

From the above discussion and visualization, it can be concluded that DCT is nothing but a one-to-one mapping of N point vectors between the time and the frequency domains. This behavior of DCT introduces energy compaction in the coefficients with highly correlated data in time domain. So, correlation characteristic of input data determines whether the frequency domain has high energy concentrated in the low frequency region or not. This property helps to produce a large sequence of zeros for higher order coefficients and also in the quantization process for further processing. So, elimination of some high frequency content has little impact on significant quality degradation of the reconstructed signal. To enhance the energy compaction property of DCT, segmentation (QRS, P and T sections) of ECG data can be performed in time domain. Then a combination of the quantization and linear

encoding can improve the efficiency of the compression of DCT coefficients. The aforementioned attributes of the DCT have led to its widespread deployment in data compression. Normally compression schemes that uses any kind of transformation, integrates a type of approximation to the compressor. This is known as quantizer and the system helps to reduce variations among transform coefficients.

4.3 Quantization

The quantization reduces redundancy in the DCT coefficients and also the number of bits required to encode coefficients. Thus the process can be defined as mapping of Q from an input set X to an output set C such that the ordinality (number of bits) of C is smaller than that of X .

It maps the input $x = \{x_i\}, x_i \in X$, to an output $q \in C$, where q is a quantization index taken from the set of quantization indices C . If x contains only one element, then this operation is called scalar quantization and it is called vector quantization if x contains more than one elements. By its very nature, quantization is a non-invertible function and is mainly responsible for the loss of information or distortion.

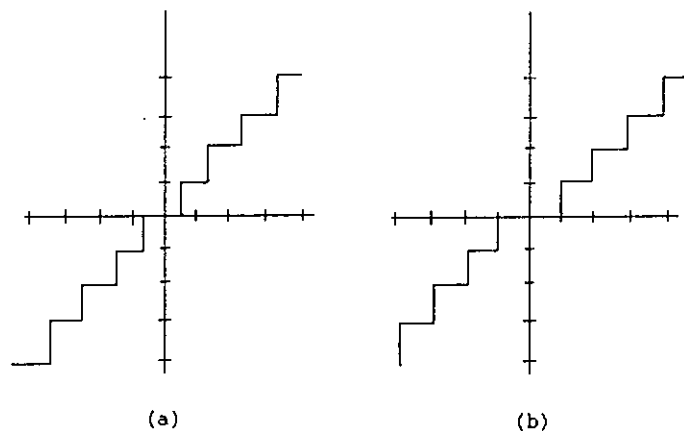


Figure 4.2: Graphs of simple quantizer functions (a) rounding function,
(b) Truncation function

Threshold function $\Theta(x)$ returns x if $x \geq \theta$, where $\theta \in R$ a threshold value and it returns zero otherwise. Other scalar quantization methods include: (a) rounding

function which returns nearest integer to its argument and (b) truncation function which returns only integer parts of its argument.

The output of $\Theta(x)$ may usually be rounded to the nearest integer in order to reduce the ordinality (number of elements) of C . Such quantizers are of great importance for both signal and image coding because they produce zero output for small input values. Here scalar quantization is chosen over vector quantization because of the memory and speed requirements of affordable tele-cardiology workstations.

Rounding the output values of threshold function returns two type of output: zero and non-zero integer values greater than θ in magnitude. This simple modification helps to feed the output of quantizer directly to an entropy coder. Entropy coding is designed so that the numbers that are expected to appear most often in integer sequence need the least amount of space in coder output. Then data compression is achieved by replacing each fixed-length input symbol by the corresponding variable-length prefix codeword. An example of the entropy encoding is the Huffman coding. In this research work this type of coding is used to encode the length of long redundant input sequences.

Chapter 5

PREPROCESSING OF ECG SIGNAL

A significant part of most of the ECG signals analysis and compression schemes are the identification of the various waves and complexes (PQRST features) presents in the signal. Among the feature detection processes, QRS detection is the predecessor of all. R wave helps to detect and classify other features like P and T waves, ST segment classification, baseline removal and etc. So, QRS detection plays a vital role in ECG signal preprocessing and it should be done first.

The database used in this work is a collection of files from the MIT-BIH Arrhythmia Database. Each signal file contains two channels of ECG signals sampled at 360 Hz. Each sample is represented by 11-bit two's complement amplitude. Mean noise value is removed from these 360 Hz sampled raw ECG data by applying mean reduction. Then these files are resample at 250 Hz, in order to fit the compression and the feature extraction algorithms. Then to extract the amplitude, shape and duration features for measuring the WDD index and also the compression ratio of our proposed algorithm, we have applied some preprocessing to the resample ECG data (P, QRS, and T sections).

The compression algorithm also uses other diagnostic features for comparing the compressed beat signal (after reconstruction) and the original beat. So, the main effort of feature extraction is finding the exact location of the characteristic parameters as shown in Figure 5.1 [13].

After finding the waves' locations, the determination of the wave's amplitudes and shapes is much simpler. The strategy for finding the waves' locations is to first recognize the QRS complex, which has the highest frequency components. T wave is recognized next, and, finally, the P wave, which is usually the smallest wave. Then the baseline and the ST features are relatively easily estimated.

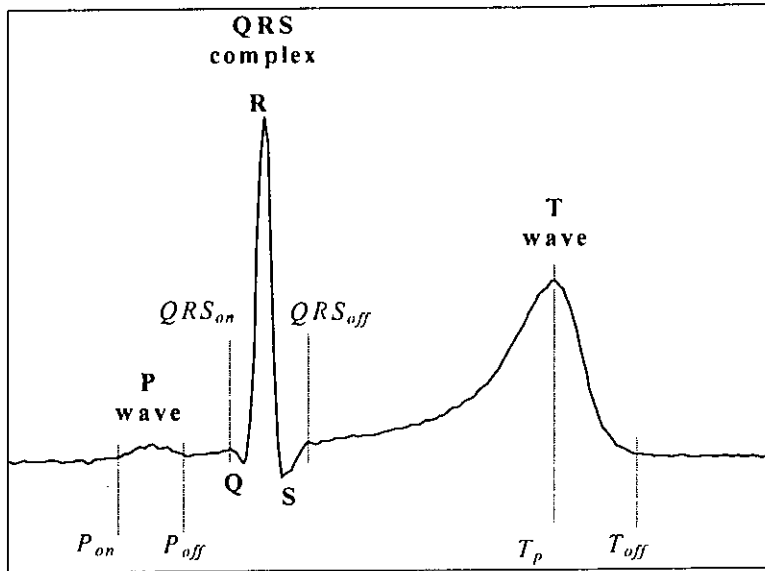


Figure 5.1: PQRST complexes location points of one beat

5.1 QRS detection

The detection of QRS complexes is the basis of ECG processing applications such as rhythm analysis, feature recognition (P, QRS, T) and ECG compression. The main challenges in QRS detection lie in patterns with varying morphology, large P and T waves, and different types of artifacts and noise. A general scheme for QRS detector consists of three steps: 1. Coarse QRS limits determination, 2. Peaks and notches determination, and 3. Exact limits determination [13]. The block diagram of three stage QRS detection process is shown in Figure 5.2.

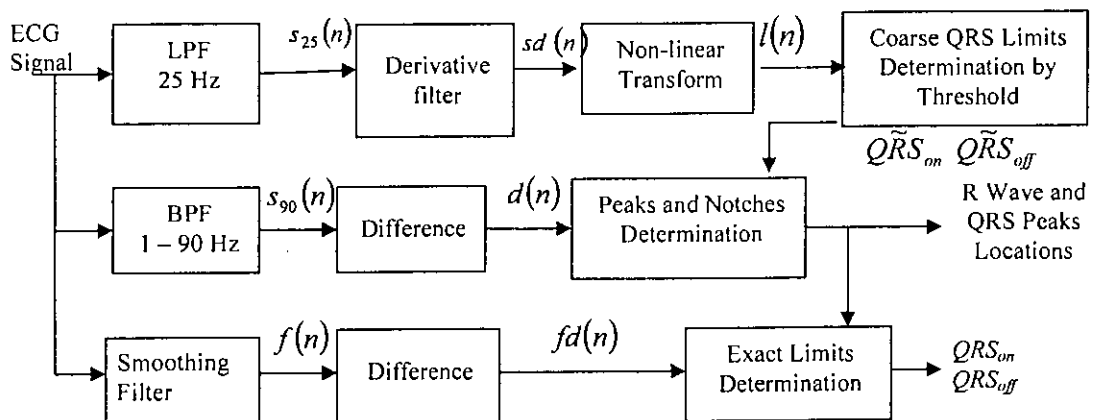


Figure 5.2: Simplified block diagram of the QRS detector

Step 1: Coarse QRS limits determination - The ECG signal is first filtered with a 25 Hz low pass filter to eliminate noise that might influence the detection algorithm. Then a derivative filter is applied to the filtered output. The equation of the derivative filter is:

$$sd(n) = (s_{25}(n+1) - s_{25}(n-1)) / 2 \quad (5.1)$$

After applying derivative filter, ECG data is passed through a moving average filter with the help of a non-linear transform. The equation of the non-linear transform is:

$$l(n) = \sum_{i=-k/2}^{k/2} sd(n+i) \quad (5.2)$$

The window size k of the average filter is determined by the average width of QRS complex. Here value of k is used as 25.

To determine the coarse limits of the QRS complex, we threshold moving average filter's output. Normally threshold level determination is dependent on the previous epoch of the nonlinear transformed signal. But, due to excessive amount of high frequency noise or movement artifact, this type of coarse limit detection may fail as sudden increase in $l(n)$ may not be dependent on the previous epoch. So, here we have used not only the maximum epoch as a standard but also the mean of all the filtered coefficients is added to the maximum.

Thus, the values of the variable *thresh* are determined heuristically:

$$thresh = ((0.5 \times \max(l(n)) + \text{mean}(l(n)))) / 2 \quad (5.3)$$

Here, false coarse limits caused by T waves and artifact are rejected.

Step 2: Peaks and Notches determination - The ECG signal is re-filtered using 1 – 90 Hz band pass, and differenced. The difference operation has the transfer function:

$$H_d(z) = \frac{z^{+1} - z^{-1}}{2} \quad (5.4)$$

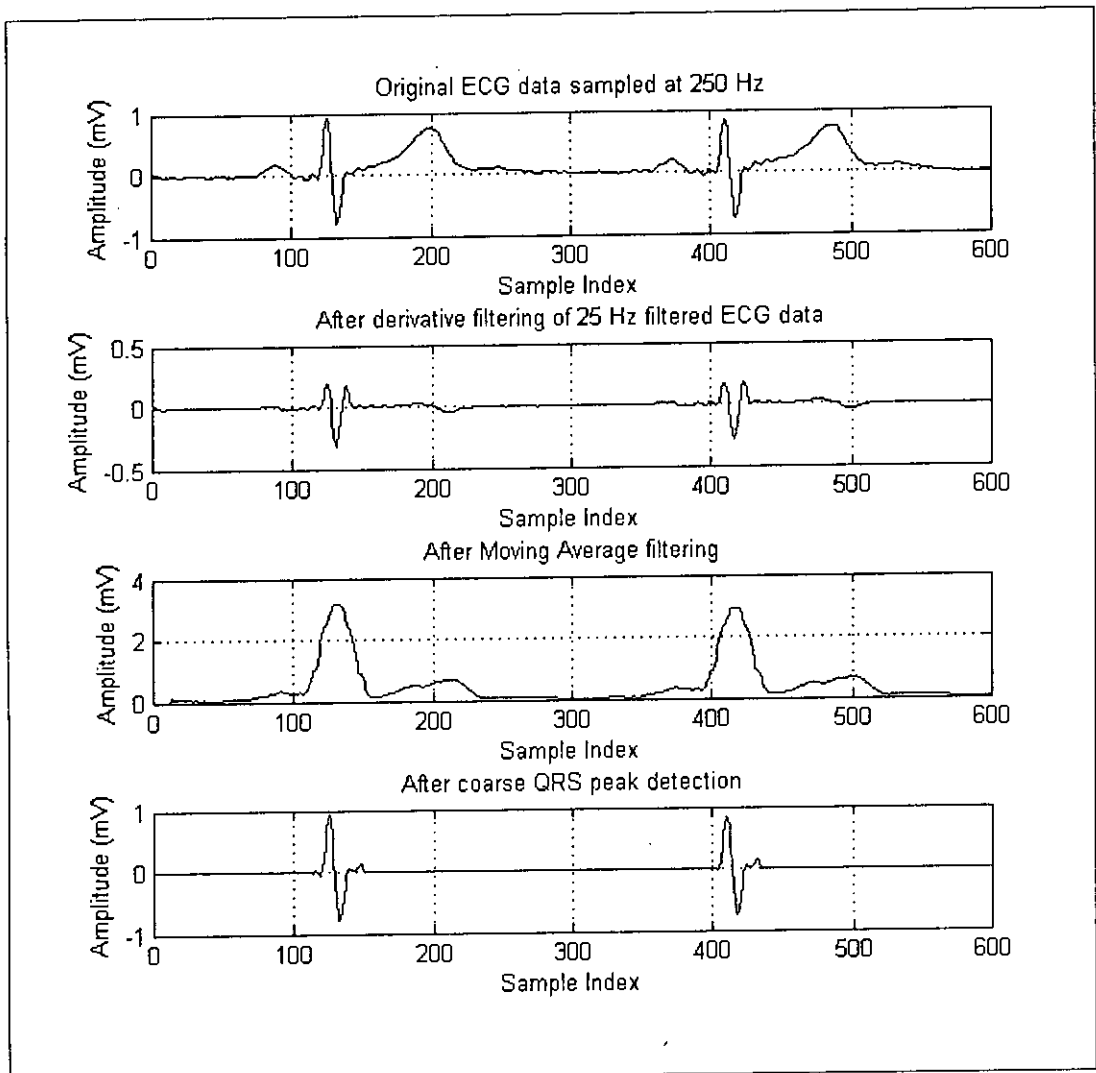


Figure 5.3: The QRS complex coarse limits estimation process

The differenced signal $d(n)$ is used to find the R wave and other peaks and notches in the QRS complex (if they exist). This is done by defining a derivative threshold d_{th} for each complex, which is calculated with this equation:

$$\begin{aligned}
d_{\max} &= \max_{\tilde{QRS}_{on} \leq n \leq \tilde{QRS}_{off}} \{d(n)\} \\
d_{\min} &= \max_{\tilde{QRS}_{on} - 30 \leq n \leq \tilde{QRS}_{on}} \{d(n)\} \\
d_{th} &= 1.05 \times \max \left\{ d_{\min}, \frac{d_{\max}}{20} \right\}
\end{aligned} \tag{5.5}$$

The factor 1.05 that is used to calculate the d_{th} might be varied depending on the variations in the height of QRS for different database as the original ECG signal often suffers from baseline wander noise. The output will have constant baseline with exaggerated high frequency components. Thus, noise level can be estimated by looking at the isoelectric part of the output signal. Two thresholds are applied to the differentiated signal $d(n)$ to determine the positions of the peaks and notches of the ECG signal and they are identified by +1 or -1 of $pne(n)$ using the equation:

$$pne(n) = \begin{cases} 1 & \text{if } d(n) \geq +dth \\ 0 & \text{if } -dth < d(n) < +dth \\ -1 & \text{if } d(n) \leq -dth \end{cases} \tag{5.6}$$

The peaks and notches locations in the QRS complex are determined by the locations of the zero crossing of the $pne(n)$ signal as shown in Figure 5.4 (c), inside the search interval. The size of the interval is controlled by the coarse limits of the QRS complex (\tilde{QRS}_{on} and \tilde{QRS}_{off}). The first positive wave in the QRS complex in the QRS complex is defined as R wave.

Step 3: Exact limits determination - The exact limits of every QRS complex are determined by first filtering the ECG signal by a smoothing FIR filter with the transfer function:

$$H_{sf}(z) = (z^{-2} + 2z^{-1} + 3 + 2z^1 + z^2)/9 \tag{5.7}$$

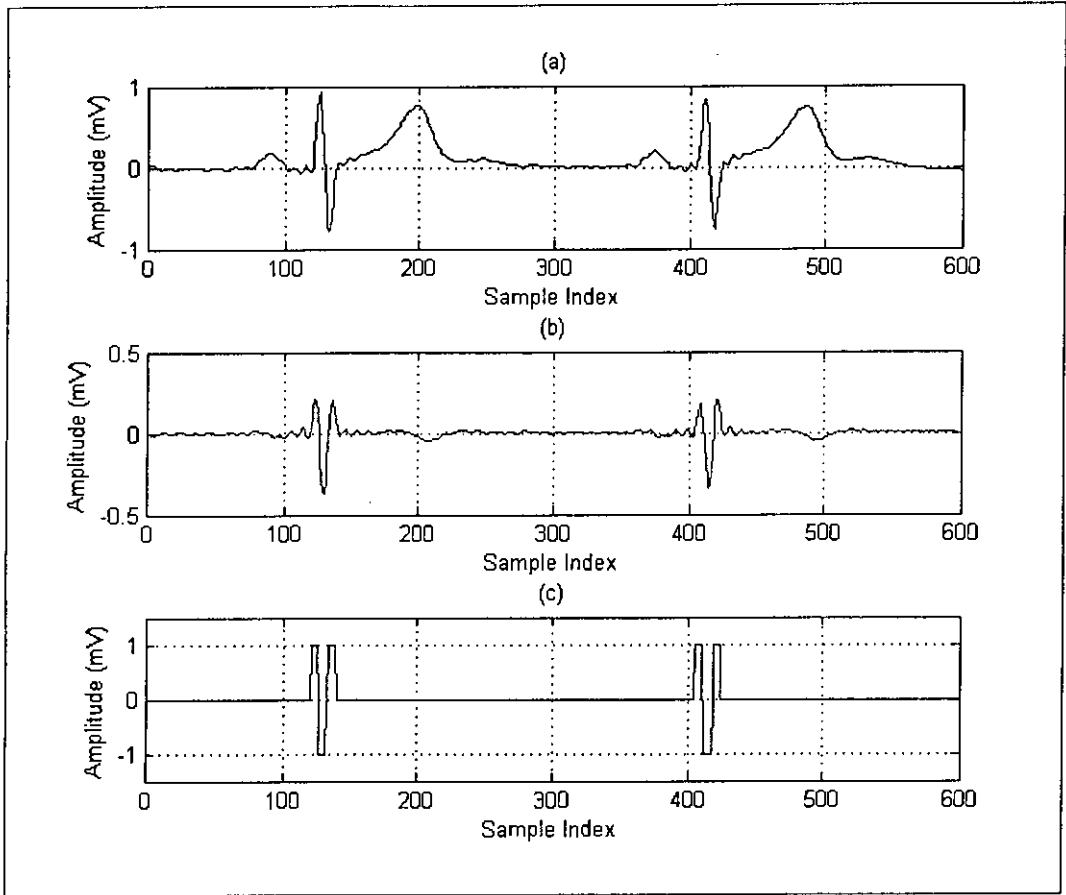


Figure 5.4: The estimation process of peaks and exact limits of one QRS complex
 (a) Two beat of ECG signal (b) The derived signal $d(n)$
 (c) $pne(n)$ that emphasizes on the locations of peaks and notches

and then differentiating the smoothed signal ($fd(n)$). Two thresholds are then calculated:

$$th_{on} = \frac{\max_{QRS_{on} \leq n \leq \text{first peak}} \{fd(n)\}}{10} \quad (5.8)$$

$$th_{off} = \frac{\max_{\text{last peak} \leq n \leq QRS_{off}} \{fd(n)\}}{10} \quad (5.9)$$

The locations are identified as the exact onset and offset of QRS complex by the following equation:

$$fd_{on} = \arg \max_{QRS_{on} \leq n \leq \text{first peak}} \{fd(n)\} \quad (5.10)$$

$$fd_{off} = \arg \max_{last\ peak \leq n \leq QRS_{off}} \{fd(n)\} \quad (5.11)$$

The exact limit of the QRS onset QRS_{on} is targeted as the first sample of $fd(n)$ that is less than the threshold th_{on} (from fd_{on} and backward) and the exact limit of QRS offset QRS_{off} is the first sample of $fd(n)$ that is less than the threshold th_{off} (from fd_{off} and forward).

5.2 T wave detection

T wave always appears after the QRS complex and can have various shapes. In this section we are going to detect the peak T_p and the offset of T wave T_{off} along with the shape of the wave T_{shape} . Three shapes are to be considered for T wave: positive, negative, and flat. The detection algorithm is based on [13]. 250 Hz sampled ECG signal is given to the T wave detector along with the locations of the QRS complex offset (QRS_{off}) and the R wave that are estimated by the QRS complex detector. The whole T wave detection process is shown in Figure 5.5 by using simplified block diagrams.

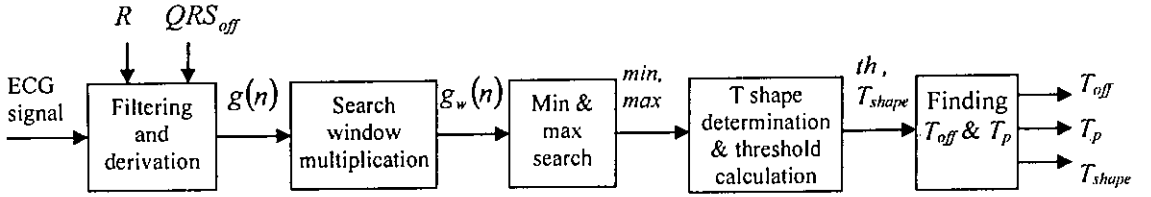


Figure 5.5: Simplified block diagram of the T wave detector

The ECG signal is filtered and differentiated, by a filter with a transfer function:

$$H(z) = \frac{(1 - Z^{-6})(1 - Z^{-8})}{1 - Z^{-1}} \quad (5.12)$$

The derived signal $g(n)$ is multiplied by a search window, which has the equation:

$$win(n) = \begin{cases} 1 & ; R + bw \leq n \leq R + mw \\ 1 - \frac{n - R - mw}{ew - mw} & ; R + mw \leq n \leq R + ew \\ 0 & ; \text{else} \end{cases} \quad (5.13)$$

where bw , mw , and ew are the beginning, middle and end points of the window respectively. Their value depends on the average value of the RR interval ($RRav$):

$$bw = \begin{cases} 120msec & RRav > 700msec \\ 100msec & RRav \leq 700msec \end{cases}$$

$$ew = \begin{cases} 500msec & RRav > 700msec \\ 0.7RRav & RRav \leq 700msec \end{cases}$$

$$mw = 0.8(ew - bw)$$

This window is shown in Figure 5.6 (b). The slope of the window is used to reduce large and close P waves. The search for maximum and minimum values is made over the multiplied derived signal $g_w(n)$ as shown in the Figure 5.6 (d).

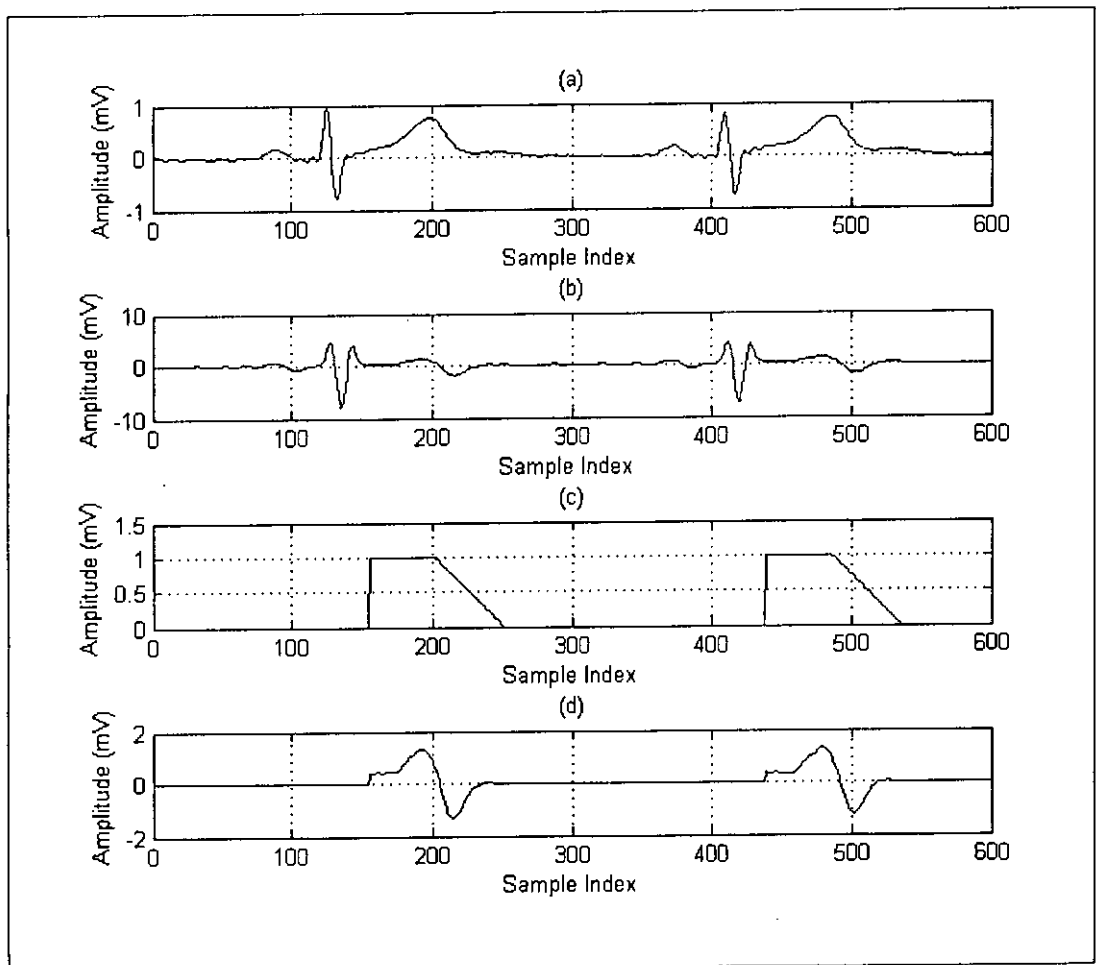


Figure 5.6: T wave detection (a) The input ECG signal (b) The derived signal $g(n)$ (c) The search window (d) The multiplied derived signal $g_w(n)$ by the search window.

Shapes of T waves are determined as follows: **positive** – if *max* before *min*, **negative** – if *min* before *max*. The threshold *th* for finding the T offset T_{off} is calculated using the equation:









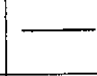
$$th = \begin{cases} g_w(min)/2 & \text{if } T \text{ is positive} \\ g_w(max)/2 & \text{if } T \text{ is negative} \end{cases}$$

The T_{off} point is determined to be the threshold crossing point. The T_p is determined to be the zero crossing point between the *min* and *max* points. T wave is determined to be flat if the difference amplitude between T_p and T_{off} is less than 1mm (1mm = 0.1mV).

5.3 P wave detection

Normal duration of the P wave is about 100 msec and appearance is before QRS complex. P wave is usually the smallest wave in the ECG signal that makes P wave detection a difficult task. The algorithm used in this work is from [13]. Table 5.1 shows the possible nine shapes of P wave that can be estimated by the P wave detector.

Table 5.1: P wave shapes

								
negative	positive	biphasic I	biphasic II	notched positive	notched negative	pulmonale positive	pulmonale negative	flat

The block diagram of the P wave detector is shown in Figure 5.7.

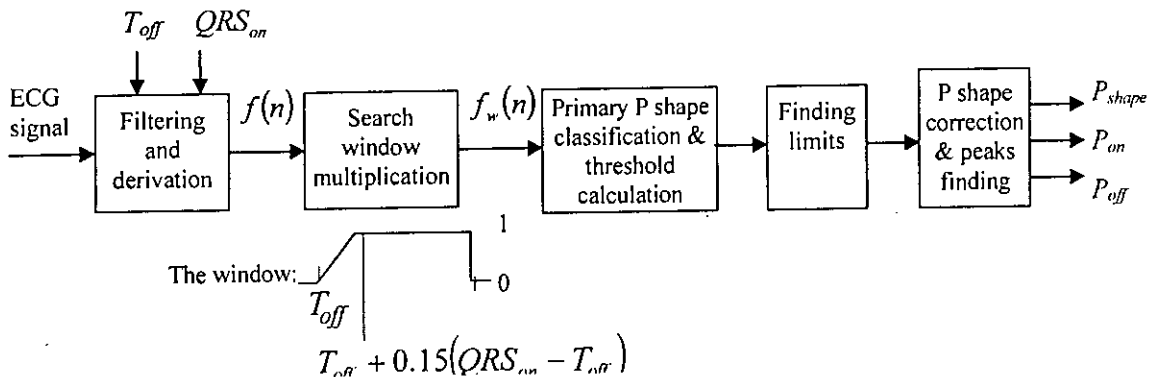


Figure 5.7: The block diagram of the P wave detector

The input to the detector is the ECG signal and the location points of QRS_{on} of the current beat and T_{off} of the previous beat. The ECG signal is filtered with a band pass filter of 0.01 – 30 Hz and differenced, before it is given to the detector. Then the differenced signal $f(n)$ is multiplied by a search window and the temporal shape of the P wave is determined.

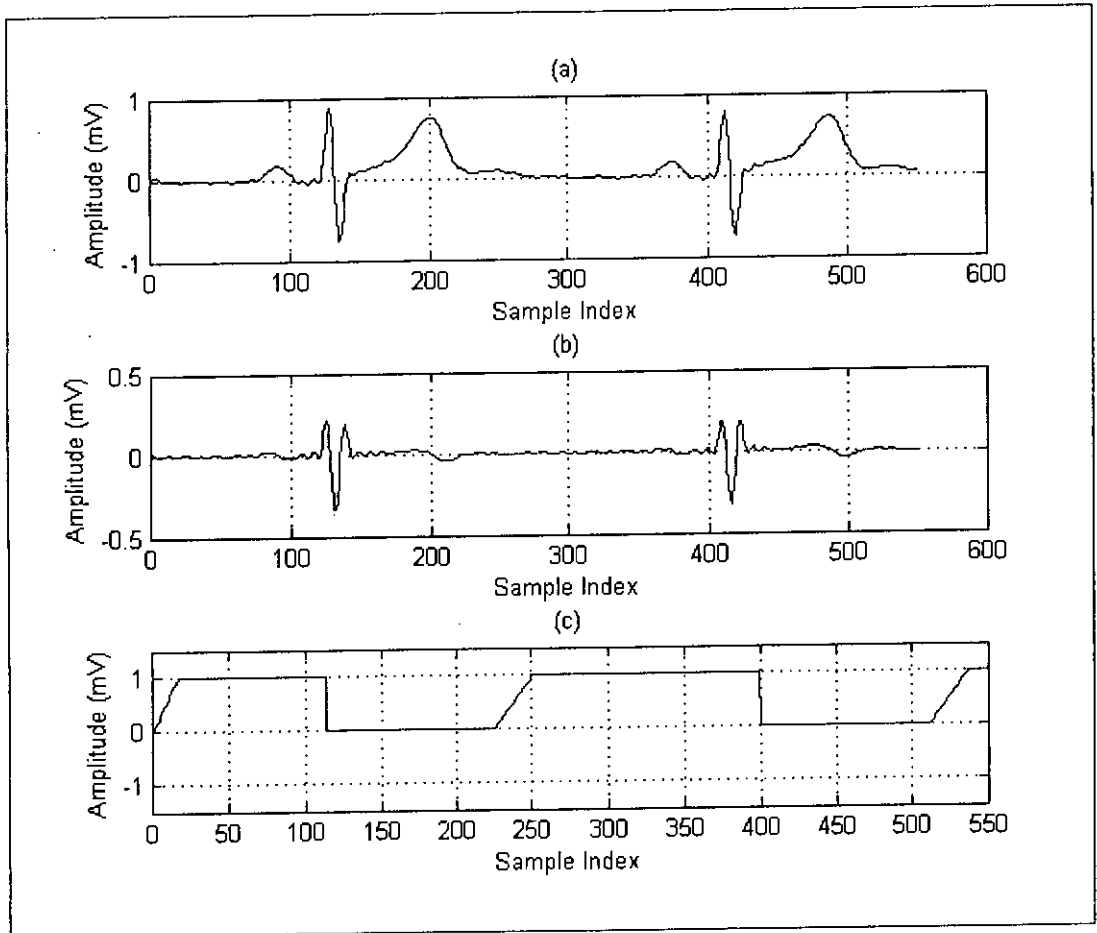


Figure 5.8: P wave detection (a) The input ECG signal after band pass filtering $f(n)$
 (b) The derived signal $fw(n)$ (c) The search window

The algorithm for P shape classification P_{shape} consists of three stages: 1. primary classification, 2. edge of P wave detection, and 3. final classification with peaks and notches detection. The flow chart of the primary P shape classification is shown in Figure 5.9.

After the primary P shape determination, the limits of the P wave (P_{on} , P_{off}) are estimated by a similar process as used for the QRS exact limits estimation with a threshold value that is 5 times less than the derived signal peaks max , max_L/min_L , max_R/min_R at the edges. P shape decision correction is performed after the limits estimation with the procedure shown in the flow chart in Figure 5.10. The peaks and notches locations are determined by the zero crossing of the derived signal $f_w(n)$ between the P limits (P_{on} , P_{off}).

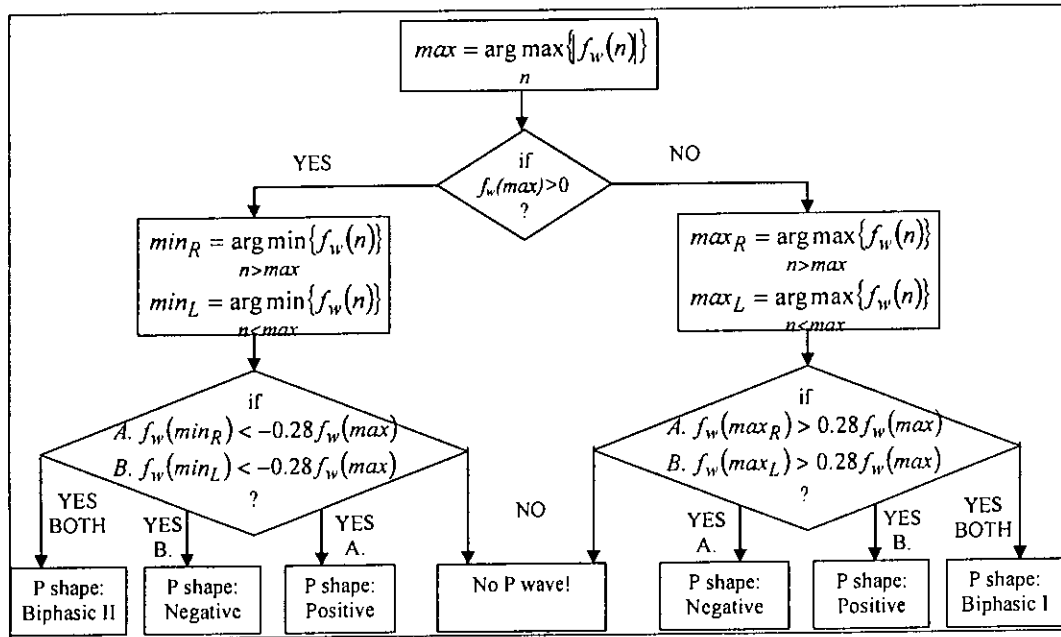


Figure 5.9: The flow chart of the primary P shape classification

5.4 Baseline Estimation

Normally the baseline is characterized by low frequency noise (baseline drift) on which the ECG signals is rides on as shown in Figure 5.11.

The Base Line can be extracted in three stages:

1. For every ECG beat that includes a P wave, a 32msec window with minimum variance is searched in the interval $[P_{off}, QRS_{on}]$.

2. In this window the mean is calculated and a point in the center of this window with the value of the mean is denoted (BLP_i).

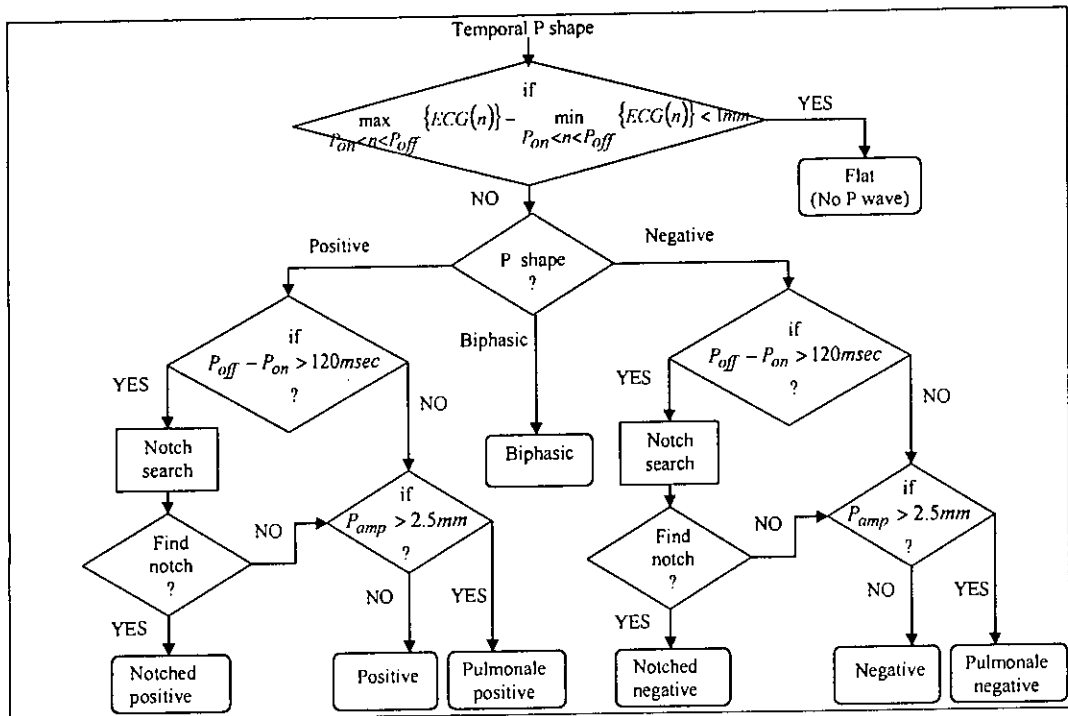


Figure 5.10: The flow chart of the P shape decision correction

3. Making a first order interpolation with these points (BLP_i , $i=1,2,\dots$, number of complexes with P wave). The process of estimation of baseline is shown in Figure 5.11 [13]. The circles are the BLP_i points.

After Base Line removal from the ECG signal, all the amplitude features are recalculated. All processing demonstrated graphically above, are calculated after baseline removal from original ECG signal.

5.5 ST Segment Features

In the ST segment, three features are extracted: **ST elevation**, **ST slope**, and **ST shape**. The process begins with determining the location of the ST point as shown in Figure 5.13. The location of the ST point is dependent on the heart rate. So, if the heart rate is slower than 60 bpm, then the ST point is placed 80msec after QRS_{off} .

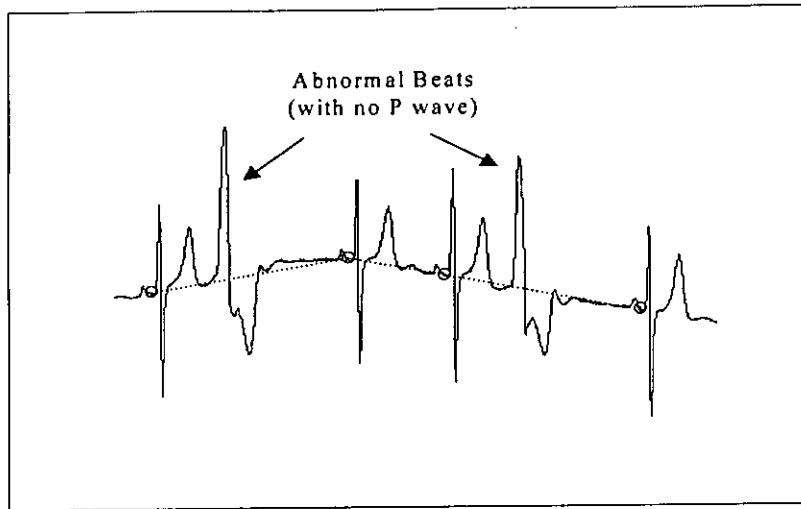


Figure 5.11: ECG signal with baseline drift
(The dashed line is the estimated baseline)

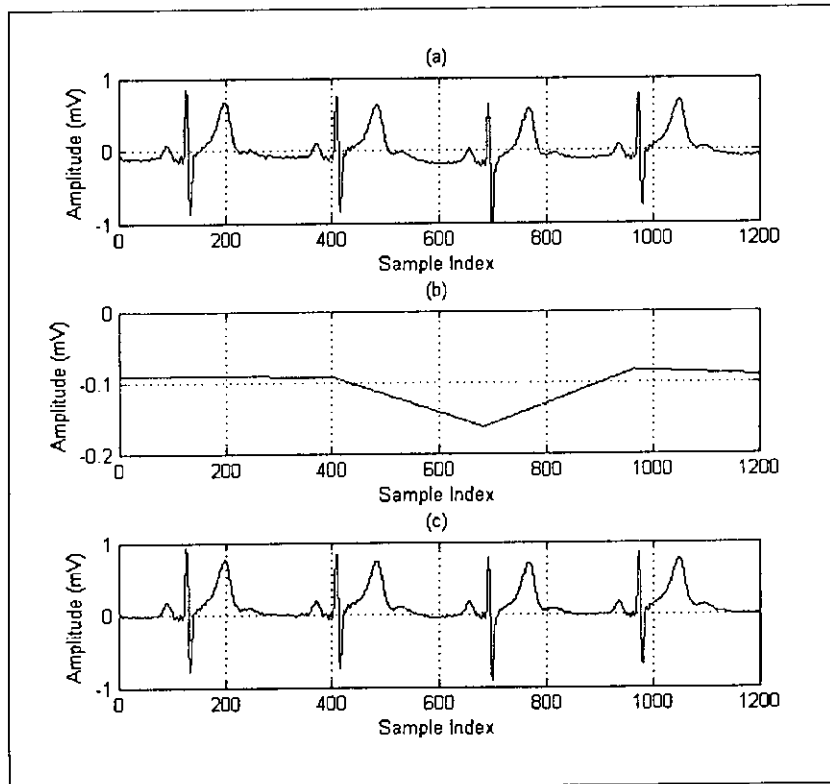


Figure 5.12: Baseline Estimation of ECG signal
(a) ECG signal before baseline removal
(b) Estimated baseline
(c) ECG signal after baseline removal

Again, if the heart rate is faster than 60 bpm, then the ST point is placed 60msec after QRS_{off} . The **ST elevation** is the amplitude of the ST point. The **ST slope** is the slope in mm/sec units of the ST point relatively to QRS_{off} as indicated by the J point. The **ST shape** is one of five shapes: flat, concave, convex, straight positive and straight negative. The ST shape is determined using a very simple algorithm, which compares the amplitudes of three points: 1. the point that is distant 60 msec before the ST point, 2. the ST point, and 3. the point that is distant 60 msec after the ST point. If the maximum difference between the amplitude of these three points is less than 1mm, the shape is determined to be flat.

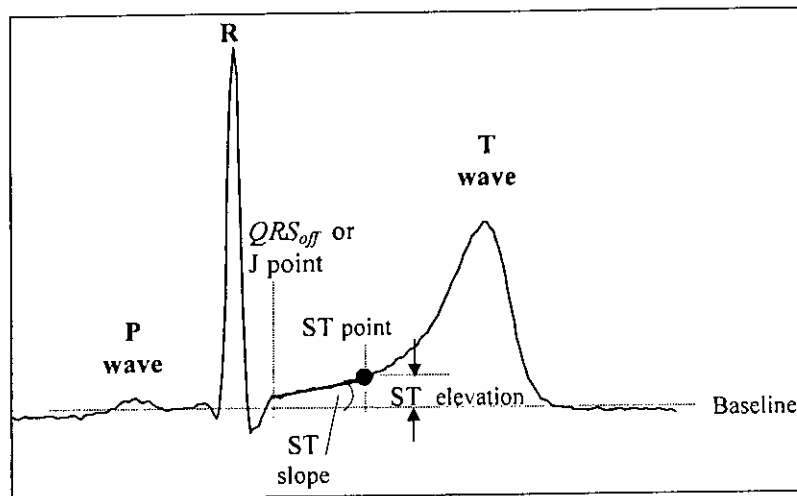


Figure 5.13: The ST segment features

Chapter 6

PROPOSED ALGORITHM AND RESULTS

This chapter contains the detailed description of our proposed RLE based compression algorithm. It performs RLE on the length of redundant sequences of DCT coefficients and then uses Huffman coding of the RLE values for digitization. The compression can be considered as a hybrid of the transformation techniques and parametric extraction techniques. Also, this chapter presents the results obtained by the proposed scheme and evaluates its performance with some existing techniques in literature. To evaluate our scheme with some other well known compression standards, we have utilized a NN based ECG compressor. Throughout the evaluation, our main target is to explore and emphasize on the idea of using clinical diagnostic features of ECG signal as a tool for performance comparison. To meet our desired goals, we have pre-processed and prepared the input data so that calculation of PRD, WDD, RMS distortion indices can be performed easily.

6.1 Proposed Algorithm

In this section, we describe the proposed compression algorithm whose block diagram is shown in Figure 6.1. The long ECG record is first divided into segments QRS region and non-QRS regions. The segmentation is indicated by the locations provided in Figure 6.3. Then each segment is passed through the transform process. After that, the resulting DCT coefficients quantized using linear quantizer. This quantization helps to introduce redundancies into the DCT coefficients. After that, the quantized DCT coefficients are encoded using RLE algorithm that accumulates the consecutive sequences of similar coefficients. In ECG signal processing, we are allowed to lose some redundant information by quantization. This affects the quality of the signal's reconstruction. The ability of diagnosis of the recovered signal controls the amount of allowed distortion introduced by quantization. In the following subsections, detailed descriptions of the process of our ECG compression algorithm are given.

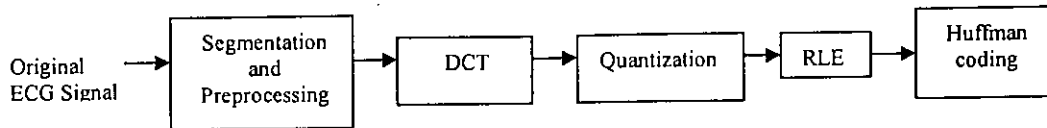


Figure 6.1: Block diagram of our proposed compression scheme

6.1.1 ECG Segmentation

To utilize the correlation property of DCT, here, quasi-periodic characteristics of ECG signal is used. This property reveals that there exists correlation between adjacent or neighbor ECG beats (inter-beat correlation) and correlation between adjacent samples (intra-beat correlation) of ECG signal according to Figure 6.2 [13]. It is observed that for inter-beat correlation, high correlation peaks exists in every RR time lag. Also, Figure 6.2 (c) shows a high correlation between adjacent samples for intra-beat ECG signal and it becomes the worst at R wave peaks.

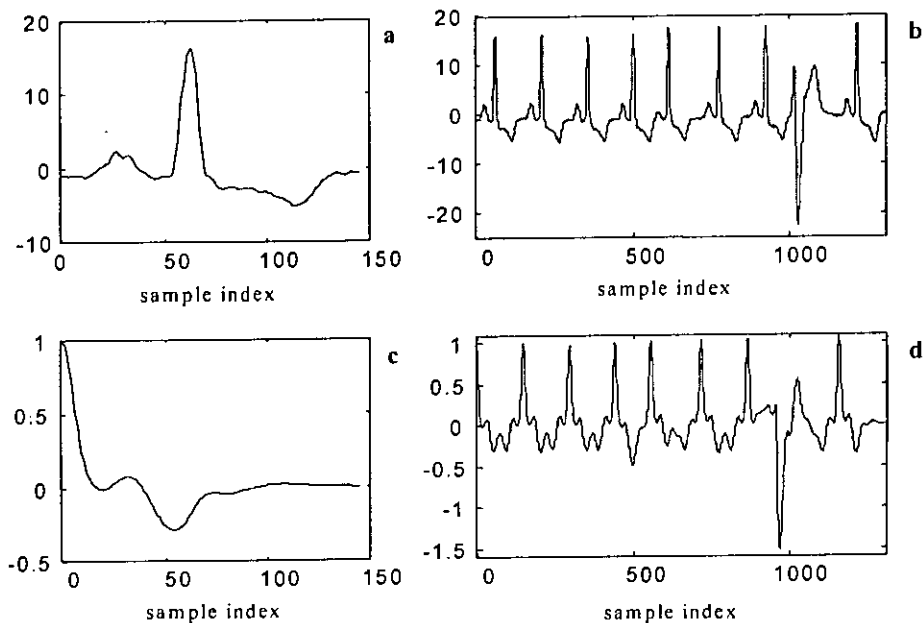


Figure 6.2: Inter- and intra-beat correlation (a) One beat (b) ECG signal (c) Intra-beat correlation (d) Inter-beat correlation (correlation between (a) and (b))

To utilize this correlative behavior among ECG beats, there should be two separate regions: the high correlated non-QRS region and low correlated QRS region. An

appropriate use of this correlation is the segmentation of ECG beats before they are converted into DCT coefficients. This will produce long sequences of zeros in frequency domain by conserving more energy in less no. of coefficients.

Depending on the high correlation between QRS and non-QRS regions, we have segmented the ECG signal into two sections: QRS complex and P and T section. To facilitate the segmentation process, the original 360 Hz sampled MIT-BIH ECG data sets are down sampled to 250 Hz. Denoising of the raw ECG signal is accomplished by mean reduction technique and baseline removal. Then segmentation of P, QRS and T features and baseline removal is performed according to [25], [13] as are described in detail on Chapter 5. Also, the indication of start and end of various segments are shown in Figure 6.3.

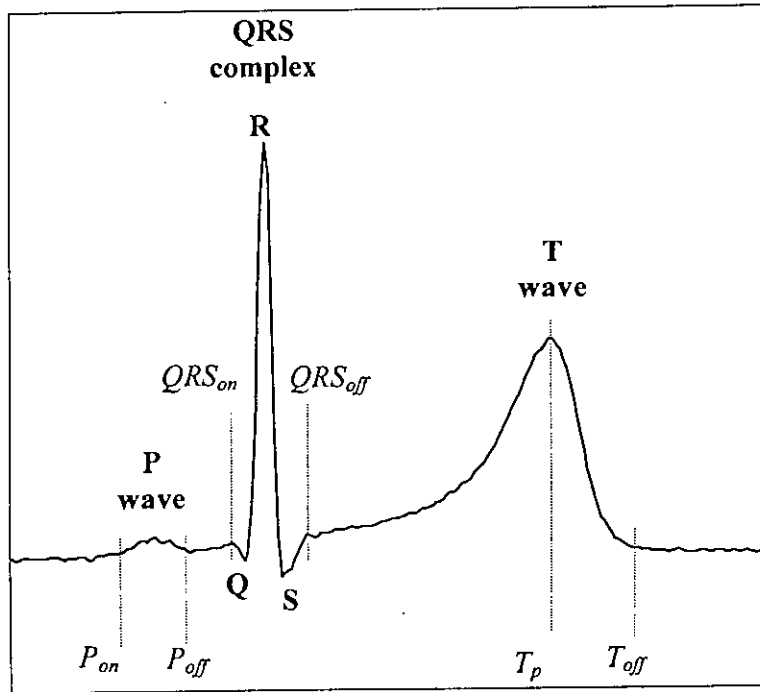


Figure 6.3: P, QRS and T features of ECG signal

6.1.2 DCT Transform

A DCT technique transforms N point data from time domain to N point coefficients in frequency domain. Each QRS-complex and P and T sections are transformed to 1-

D DCT separately. Due to the energy conservation property of DCT, it generates a long sequence of zeroes at higher frequency coefficients. Most of the energy is packed into the low frequency region. It is also verified that segmentation has a great impact on the energy conservation characteristics of DCT. But redundant use of segmentation also increases the processing complexity and the storage requirements. An optimum solution to this problem to maintain only two separate set of 1-D DCT coefficients: one for QRS-complex and the other for P and T sections. The algorithm for DCT is described in Chapter 4.

6.1.3 Quantization

Quantization plays an important role in data compression. It's an irreversible process. The amount of loss controls the no. of members in the discrete dataset that are produced after quantization. Precision of reconstruction depends on the amount of approximation or step size of quantizer. In this work, we have scalar quantized the floating point DCT coefficients both for single precision and double precision. But, we have preferred the single precision quantizer over double precision, because, with respect to CR, single precision quantization performs better and it is simple to implement. The quantizer have step size starting from 0.1 and proceeded by 0.1 until there introduces significant amount of distortion after reconstruction.

6.1.4 Run Length Encoding

The use of quantization is always motivated by the need to reduce the amount of data to represent a signal. So, the data set representing an ECG signal in terms of DCT coefficients is quantized to use redundancy encoding. By reducing the precision of the transformed values using quantization, the amount of redundancy increases, as well as the requirement of number of bits to represent the coefficients is substantially reduced.

One portion of our compression scheme is the binary representation of the run values by Equation (6.1).

$$\text{no. of symbols} \times \text{bits/symbol} \quad (6.1)$$

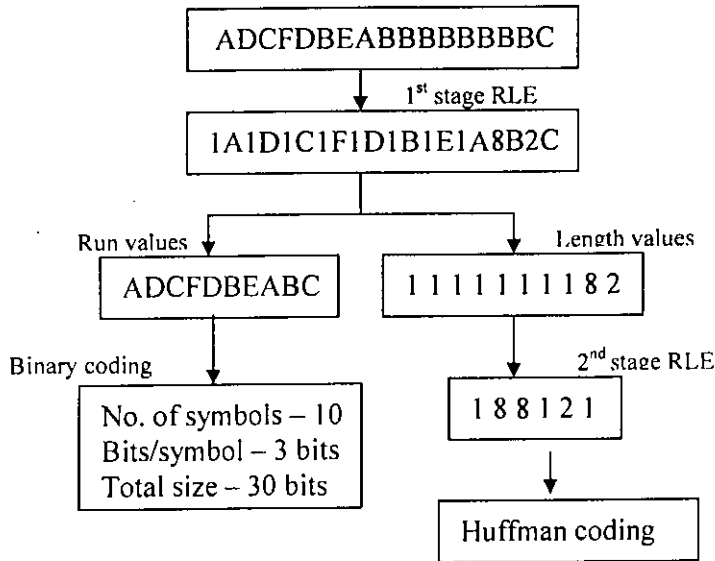


Figure 6.4: An example of our RLE based encoding scheme

Bits/symbol can be determined by the formula $\log_2 x$, where x is the no. of distinct symbols in the signal. The other portion is the result of 2nd stage RLE on lengths. Here, further data compression is possible by applying Huffman coding to the output of RLE. Also, Huffman coding is the easy method of binary encoding for any data set.

6.1.5 Huffman Encoding

Normally, discrete amplitudes of quantized signal do not occur with equal probability. So, using variable length encoding to them, depending on their frequency of occurrences, is more acceptable than fixed length encoding. Data that occur frequently is assigned a shorter code word. An example of Huffman coding scheme is presented in Figure 6.5.

Figure 6.5 reveals that at first the given data set is used to calculate the probability of occurrences and then the probabilities are used to formulate the Huffman tree. Traversal through the branches of the tree, provides a variable length code word for a symbol depending on the position of the leaf, that represents the probability of that

symbol. A left branch traversal is indicated by “1” and a right branch traversal is indicated by “0”.

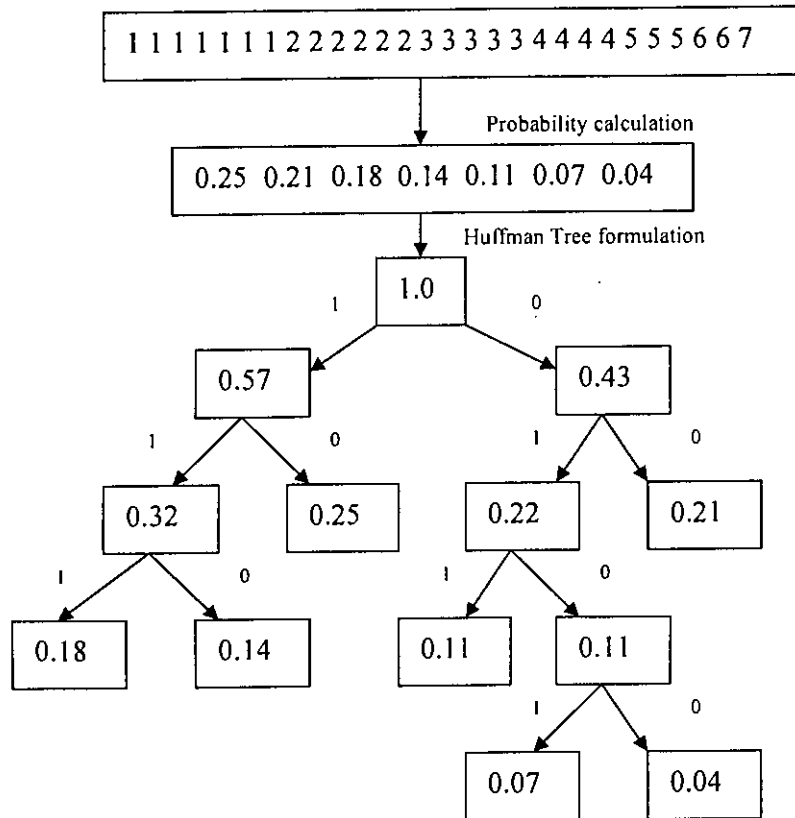


Figure 6.5: An Example of Huffman Tree formulation from a given dataset

By observing the tree, it can be concluded that, tree traversal for a code word of a particular symbol always ends at the branch that has no leaf. Now the dictionary of symbols for this Huffman coding scheme is presented in Table 6.1.

The expected code word length/bit can be calculated by Equation (6.2).

$$E[l] = \sum_{i=1}^7 l_i P_i \tag{6.2}$$

Where, l_i represents the length of Huffman code for that symbols and P_i is the probability of that symbol.

To transmit the data set in binary format, we have to replace each symbol by its equivalent code word from the Huffman dictionary. In the receiving end, to decode

the binary information, it requires the Huffman tree or the code dictionary. To retrieve the original data set, Huffman dictionary has to be sent as a header. Decoding of the binary data file is possible using the Huffman dictionary. The process always starts from the root. For each symbol, starting from the root, if a “1” is received, then we visited the left child and if a “0” is received, we visited the right child. This process continues until we get into a branch that has no child.

Table 6.1: Huffman dictionary

Symbols	Fixed length encoding	Probability of occurrence	Huffman code
1	001	0.25	10
2	010	0.21	00
3	011	0.18	111
4	100	0.14	110
5	101	0.11	011
6	110	0.07	0101
7	111	0.04	0100

A branch with no leaf indicates the finishing of a data symbol. The symbol can be decoded using the Huffman dictionary that we have transmitted as header to the binary file. This decoding continues from root for all the symbols until all the code bits are completed. For this research work, we have used two separate dictionaries: one for the QRS complexes and the other for the P and T sections.

6.1.6 Bit rate calculation

Now, the total size of our compressed ECG data file is consists of:

1. Code from the 1st stage RLE run values for each ECG beat
 - a) For P and T sections
 - b) For QRS complex
2. Code from the Huffman coding of the 2nd stage RLE values for each ECG beat
 - a. For P and T sections
 - b. For QRS complex
3. Combined Huffman code dictionary for all ECG beats

- a. For P and T sections
- b. For QRS complex

Calculation of bit rate depends on the ratio of the total compressed data bits to the equivalent time interval to generate that portion of ECG beat. We have used MIT-BIH Arrhythmia database as a test data set for our proposed compression scheme. Here, each data element is digitized using a 11-bit code word. So, we have calculated the CR of our proposed RLE based compression scheme as follows in Equation (6.3).

$$CR = \frac{N \times m}{d_p + d_q + \sum_{i=1}^n (c_{p_i} + c_{q_i} + r_{p_i} + r_{q_i})} \quad (6.3)$$

Here, N is for the no. of ECG samples (data), m is the no. of bits/data used in MIT-BIH database, d_p and d_q are the dictionary size for P and T sections and QRS complex respectively, i is the no. of ECG beats, c_p and c_q are the Huffman code size for P and T sections and QRS complex respectively and r_p and r_q are the binary code run values of RLE for P and T sections and QRS complex respectively. And bit rate is:

$$\text{Bit rate} = (\text{Total no. of bits after compression}) / (\text{Total no. of data}) \times (\text{Sampling rate})$$

6.2 Test Dataset

In order to maintain the consistency of relative comparison with other ECG data compression techniques, in this research work we have used MIT-BIH Arrhythmia database as a standard test datasets. This is a collection of 48 half-hour Holter recordings, each of which contains data from two separate ECG leads, sampled at 360 Hz with 11-bits per sample. A set of 25 records containing a variety of pathological cases was selected for testing compression performance. Appendix summarizes the major characteristics of some of the test signals. Standard limb lead II (MLII) data is commonly used in pre-hospital phase of emergency care when monitoring the heart solely for arrhythmia.

6.3 The Values of WDD Parameters

For all the results that are analyzed in this chapter, uses WDD as a distortion index to measure the compression performance. Predefined values of some characteristic

parameters for WDD are presented in this section. For the shape features (T_{shape} , P_{shape} , and ST_{shape}) of WDD as discussed in Chapter 3, the fixed penalty matrices are provided below [13].

$$W^P = \begin{bmatrix} 0 & .2 & .2 & .2 & .3 & .2 & .2 & .2 & .4 \\ .2 & 0 & .1 & .1 & .3 & .4 & .4 & .4 & .2 \\ .2 & .1 & 0 & .1 & .3 & .4 & .4 & .4 & .2 \\ .2 & .1 & .1 & 0 & .3 & .4 & .4 & .4 & .2 \\ .3 & .3 & .3 & .3 & 0 & .3 & .3 & .3 & .3 \\ .2 & .4 & .4 & .4 & .3 & 0 & .1 & .1 & .2 \\ .2 & .4 & .4 & .4 & .3 & .1 & 0 & .1 & .2 \\ .2 & .4 & .4 & .4 & .3 & .1 & .1 & 0 & .2 \\ .4 & .2 & .2 & .2 & .3 & .2 & .2 & .2 & 0 \end{bmatrix}$$

$$W^T = \begin{bmatrix} 0 & .2 & .4 \\ .2 & 0 & .2 \\ .4 & .2 & 0 \end{bmatrix}$$

$$W^{ST} = \begin{bmatrix} 0 & .1 & .2 & .1 & .4 \\ .1 & 0 & .2 & .4 & .1 \\ .2 & .2 & 0 & .2 & .2 \\ .1 & .4 & .2 & 0 & .1 \\ .4 & .1 & .2 & .1 & 0 \end{bmatrix}$$

Decoding of the specific weight for a particular shape difference between the original and the reconstructed signal from the weighting matrix is done with the help of the sequence numbers used in Table 6.2 [13].

Table 6.2: The numbering of the WDD shape features for the penalty matrices

Number Shape feature	1	2	3	4	5	6	7	8	9
P_{shape}	negative	pulmonale negative	notched negative	biphasic II	flat	positive	pulmonale positive	notched positive	biphasic I
T_{shape}	positive	flat	negative						
ST_{shape}	straight positive	concave	flat	convex	straight negative				

Diagonal weighting matrix in the present work is as follows [13]:

$$\Lambda = \begin{bmatrix} 2 & 1 & 1 & 1 & 1 & 1 & 1 & 0.25 & 0.25 & 1 & 1 & 2 & 2 & 1 & 1 & 1 & 1 \end{bmatrix}$$

6.4 Results

The effects of RLE compression on ECG signals are presented in Figure 6.6, 6.8 and 6.10 respectively by varying the step size of DCT coefficients for three MIT-BIH records. These Figures indicate that the shape, amplitude and duration of the reconstructed ECG signals are almost identical to the original signals after compression. Also, Table 6.3 illustrates the obtained compression ratios and the corresponding WDD and PRD indices with respect to the quantization resolution and bit rate for MIT-BIH record 117. By analyzing the numerical values, it is quite clear that the application of WDD as distortion measure is much better than PRD with respect to compression ratio. From literature [13], it is obtained that distortions will be in a considerable level, if we can limit our compression within 2%-4% of WDD and 6%-9% of PRD. Thus, a quantization step size of 0.2 with compression ratio 13.92 will be reasonable in the point of clinical diagnosis. So, the major portion of the ECG signals extracted from MIT-BIH arrhythmia database are tested up to the step size of 0.2.

Table 6.3: WDD and PRD variation with Quantization resolution and bit rate (bps) for Record-117

Quantization step size	CR	Bit rate (bps)	WDD (%)	PRD (%)
0.01	2.73	1007	0.0575	1.0235
0.05	6.5	423	0.3773	3.4919
0.1	10.125	271	0.455	5.9786
0.2	13.92	198	0.6362	9.299
0.4	14.866	185	2.55	15.28

Figure 6.6 shows an example of original and reconstructed ECG signal, which was compressed by the proposed compression algorithms (DCT-RLE). The original ECG signal is taken from the MIT-BIH database - record 117. Distortion indices are calculated on beat by beat basis for graphical representation of PRD and WDD with variations of CR and bit rate for a particular MIT-BIH record. For this particular record, the effects of change in bit rates on WDD, PRD and CR using our proposed compression technique are shown in Figure 6.7.

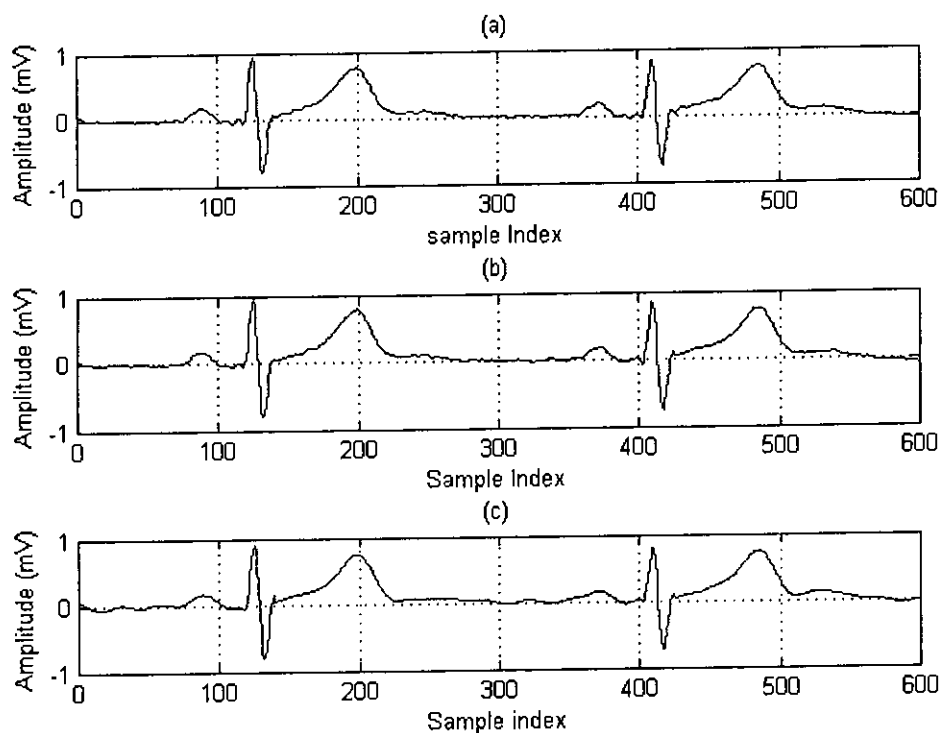


Figure 6.6: Original and reconstructed signal of record 117 (MIT-BIH)

- (a) Original signal
- (b) DCT-RLE compressor (CR 10.12, WDD 0.455%, PRD 5.97%)
- (c) DCT-RLE compressor (CR 13.92, WDD 0.636%, PRD 9.299%)

The trend of the distortion indices indicates that the bit rate below 200 bps introduces a drastic change in the quality of the reconstructed signal by the sharp upward bending. Also, the pattern confirms that WDD is less sensitive than PRD on variations of the bit rate. In reality, as WDD deals with the relevancy of the distortion

with respect to the clinical acceptability, instead of mathematical calculations, it remains less sensitive to the distortion. This property of WDD facilitates the compression process by offering higher compression ratio.

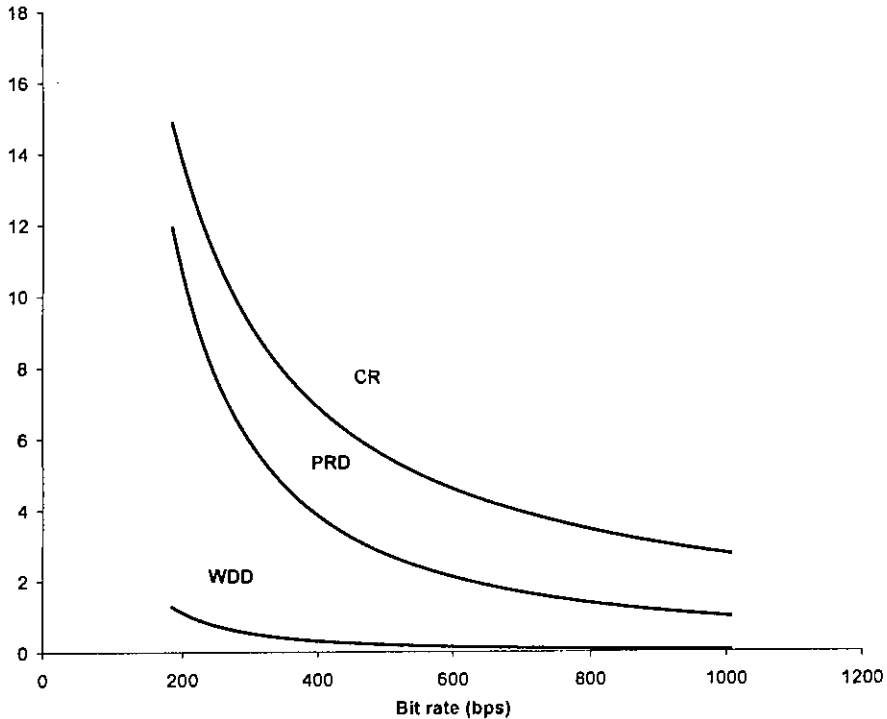


Figure 6.7: The compression ratio and distortion-rate curves of our proposed compression scheme for MIT-BIH record 117 with respect to bit rate variation

Again, for Figure 6.9, similar conclusions can be written as are in Figure 6.7. CR after 200 bps will create significant amount of distortion. The variations in the behavior of WDD for both record 117 and 119 confirm that the slope of PRD, WDD and CR vary for each record.

The trend lines of Figure 6.9 indicate that for the Record 119, our proposed DCT-RLE based scheme with WDD performs better than PRD. The variations of WDD with bit rate seem to take a sharp turn after bit rate 250 bps. This indicates that further increase in bit rate will increase the amount of distortion on the diagnostic features along with higher CR. Also, from the distortion rate curves of Figure 6.7 and

6.9, different amount of WDD index indicates the variations of the characteristics parameters of different datasets.

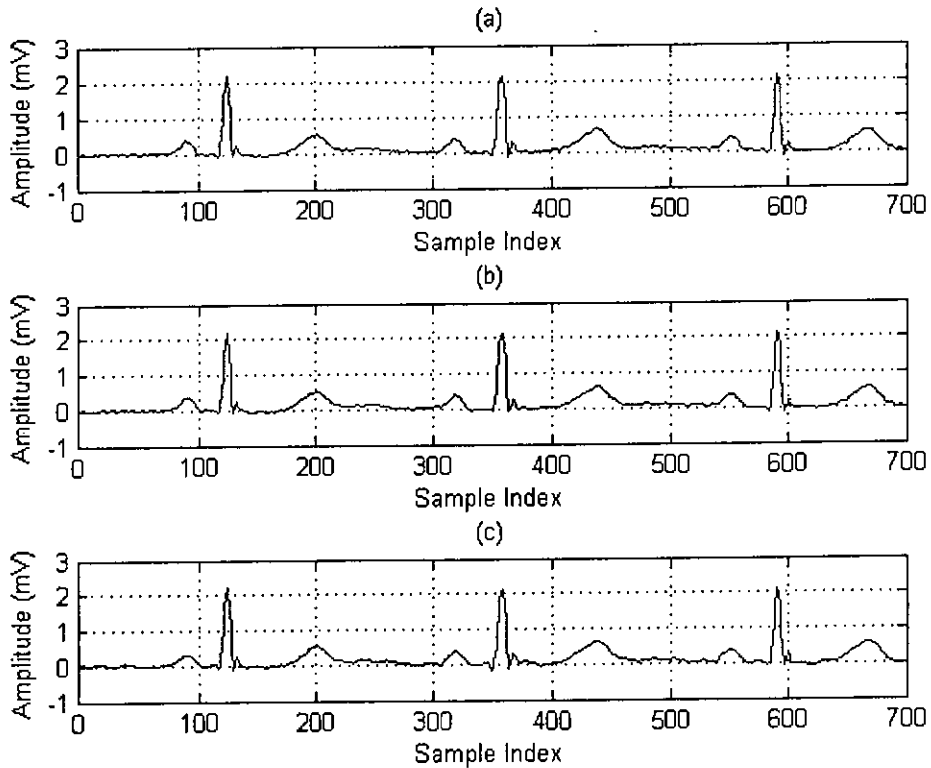


Figure 6.8: Original and reconstructed signal of record 119 (MIT-BIH)

(a) Original signal

(b) DCT-RLE compressor (CR 6.96, WDD 1.337 %, PRD 5.286%)

(c) DCT-RLE compressor (CR 8.86, WDD 2.619%, PRD 8.857%)

6.4.1 Comparison with Other Methods

The compression algorithm developed in this paper can be used for most 1-D ECG signals. However, the choices of the quantization step sizes are signal dependent. Till now, application of WDD for performance evaluation of ECG compression schemes is not explored widely. Only from [13], we have obtained some analysis on distortion measurement using WDD. These observations and analysis of the author regarding WDD are also presented in this work in Figure 6.11 to evaluate our system.

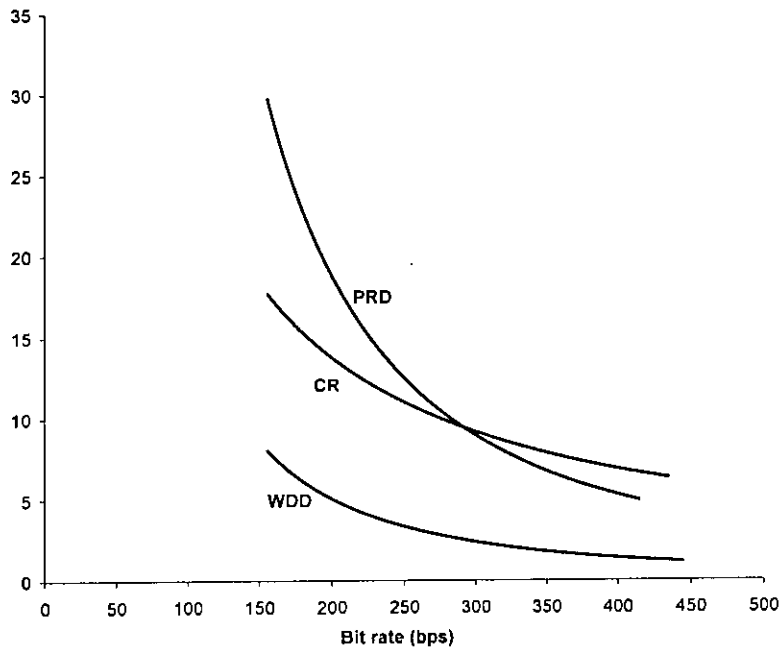


Figure 6.9: The compression ratio and distortion-rate curves of our proposed compression scheme for MIT-BIH record 119 with respect to bit rate variation

Moreover, we have used some other widely used distortion indices like PRD or RMS to evaluate our compression schemes with others in literature. It is noted that the performance of the compression algorithm depends on the particular ECG record being compressed.

From Figure 6.11, it can be observed that with respect to bit rate, LTP, AZTEC, and SAPA2 all three compression schemes represent a high distortion index than our previous results. Also, for ASECWDD, for a bit rate of 200 bps, WDD remains more than 2.5. But, for the same bit rate, our DCT-RLE based compression scheme shows less WDD than that in Figure 6.11. Further comparisons with literature are presented in Table 6.4.

Our evaluation with other compression schemes in Table 6.4 shows that our system performs much better compression than others with respect to PRD as a distortion index.

From the Table it can be observed that, 1-D and 2-D DCT based schemes in [21] have a low CR and high distortion indices with respect to our proposed DCT-RLE based compression scheme.

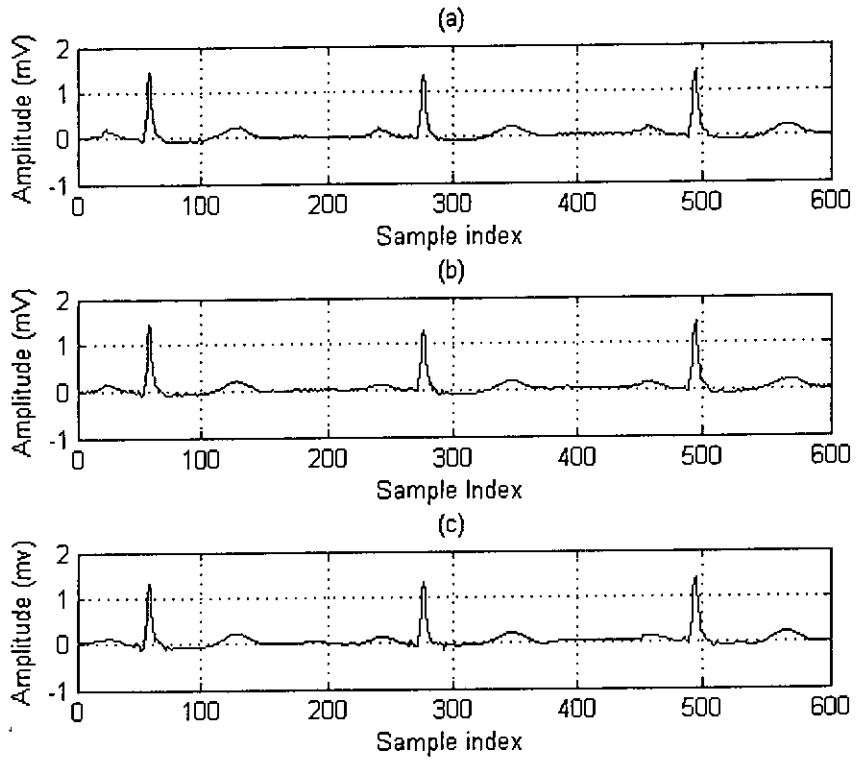


Figure 6.10: Original and reconstructed signal of record 101 (MIT-BIH)

- (a) Original signal
- (b) DCT-RLE compressor (CR 8.62, WDD 2.35 %, PRD 8.97%)
- (c) DCT-RLE compressor (CR 12.06, WDD 4.79 %, PRD 13.48%)

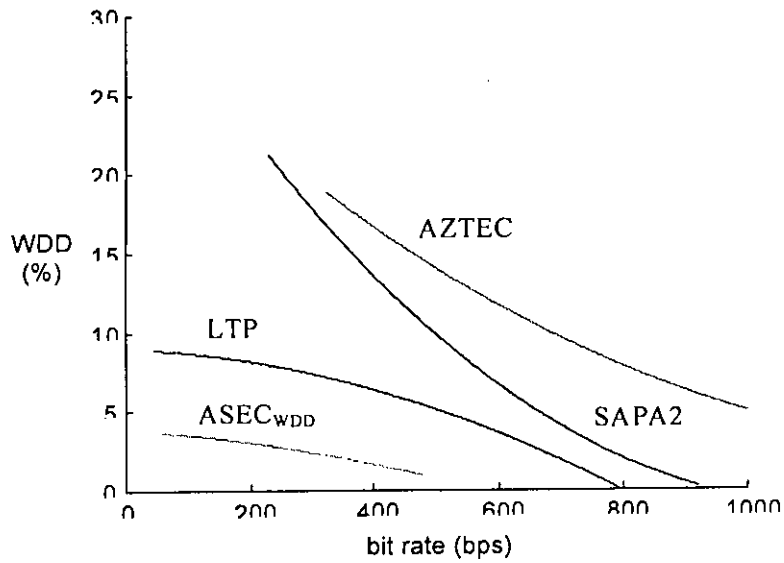


Figure 6.11: The distortion-rate curves of the algorithms: ASEC_{WDD}, LTP, SAPA2, and AZTEC

Table 6.4: WDD and PRD variation with some other techniques from literature

From literature Compressor	CR	CR _{PS}	PRD	PRD _{PS}	WDD	WDD _{PS}
AZTEC [29]	6.9	6.73	15.5	4.358	-	0.857
Long Term Prediction [29]	6.9	6.73	7.3	4.358	-	0.857
1-D DCT [21]	6.0	6.73	7.5	4.358	-	0.857
	12.0	11.39	15.0	9.087	-	1.627
Cut and align beats approach with 2-D DCT [21]	6.0	6.73	3.5	4.358	-	0.857
ASEC _{PRD} [29]	6.9	6.73	5.5	4.0	5.1	0.857

PS denotes proposed DCT-RLE based scheme.

6.4.2 Neural Network based ECG compression

Artificial Neural Network (ANN) is a special type of supervised learning system, where the main task is to determine a function from given input-output sample pairs (the training sample). The function maps any input to an output such that disagreement with future input-output pairs is minimized. A multilayer perceptron (MLP) based feed forward network with one input layer and one output layer, with one or more hidden layers is implemented here. The activation function of each neuron computes a weighted sum of all synapse inputs, subtract the sum from a predefined bias and pass the results through a nonlinear sigmoidal function whose output ranges between 0 and 1 [27]. Application of NN consists of a training phase and a testing phase. During the training phase, pattern data are applied as the input, which finally adjust the weights (w_{ij}) and bias. Here, the standard deterministic gradient-based back propagation learning algorithm is used as the training algorithm. A 3-layer neural network system with a single node for both input and output layers is presented in Figure 6.11. The activation function of the hidden layer neuron is a unipolar sigmoidal function as in Equation (6.4).

$$f(x,u) = \frac{1}{1 + e^{-x/u}} \quad (6.4)$$

where, u is the coefficient of the function. Interconnections of hidden layer with input and output layers are dependent on the weights w_{ij} . The weights are modified iteratively according to the gradients of error function using the learning rate η and momentum α as follows in Equation (6.5).

$$w_{ij}^{k+1} = w_{ij}^k - \eta \frac{\partial E^k}{\partial w_{ij}} + \alpha \cdot \Delta w_{ij}^k \quad (6.5)$$

where E^k is the k-the error term.

The learning rate of 4.88281×10^{-5} and momentum of 0.5 was configured for the ANN using Neural Simulator [28]. Segmentation is performed on each ECG beat before ANN based learning according to the preprocessing described in Chapter 5. Figure 6.12 indicates the performance of the NN based scheme.

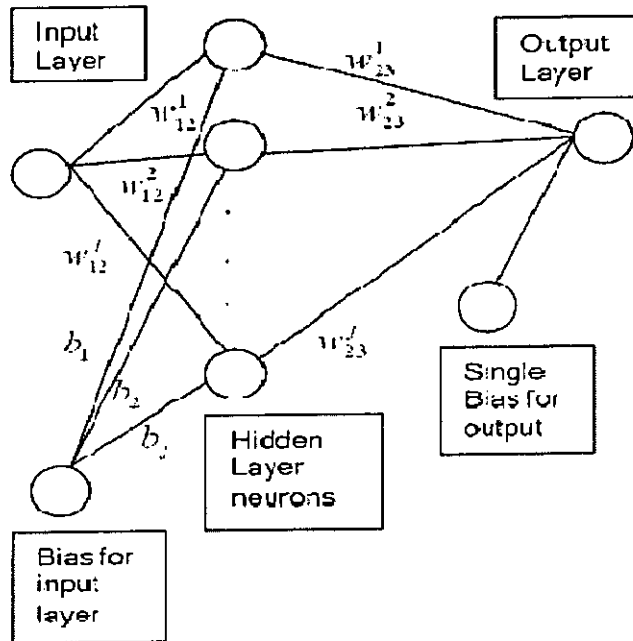


Figure 6.12: A 3-Layer Neural Network

The WDD of the reconstructed signal from the DCT-RLE in Figure 6.10 (b) is 0.455%, with an average bit rate of 271 bps, CR of 10.12 and a PRD of 5.97%. For the same MIT-BIH record our developed NN based scheme has shown a CR of 9.8 with WDD of 0.56% and PRD of 7.33%. This result indicates the superiority of our proposed compression scheme over ANN based compression. Note that, the error of the NN compressor is somewhat larger than the error of the DCT-RLE compressor in the reconstructed signal in Table 6.5 for all the presented ECG databases. Rate distortion curves both for DCT-RLE and NN based schemes are presented in Figure 6.13.

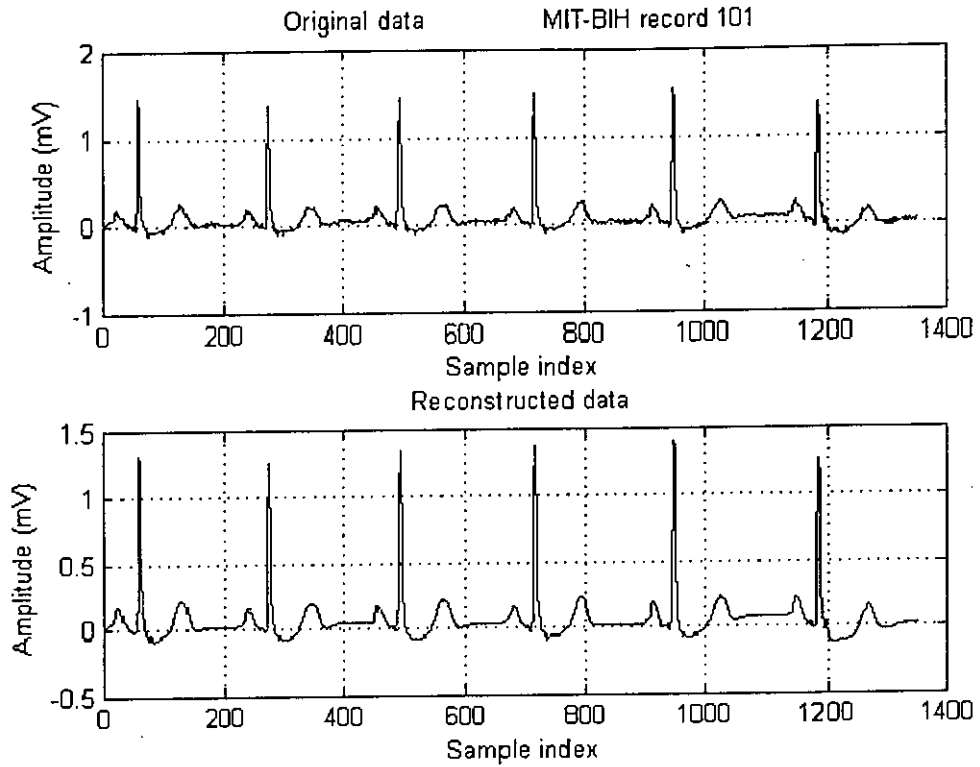


Figure 6.13: MIT-BIH record 101 after NN based compression

(CR 8.65, WDD 3.6%, PRD 10.86%)

Table 6.5: Results of WDD index, PRD and RMS errors of DCT-RLE based and NN based schemes

Performance measure	MIT-BIH Record 101		MIT-BIH Record 117		MIT-BIH Record 119	
	PS	NN	PS	NN	PS	NN
Avg. CR	8.62	6.78	13.92	9.80	8.86	6.14
Avg. WDD (%)	2.35	2.51	0.64	0.56	2.62	5.29
Avg. PRD (%)	8.97	9.57	9.29	7.33	8.86	7.99
Avg. RMS	0.016	0.0177	0.021	0.0167	0.0279	0.0192

PS denotes proposed DCT-RLE based scheme. NN denotes neural network based scheme.

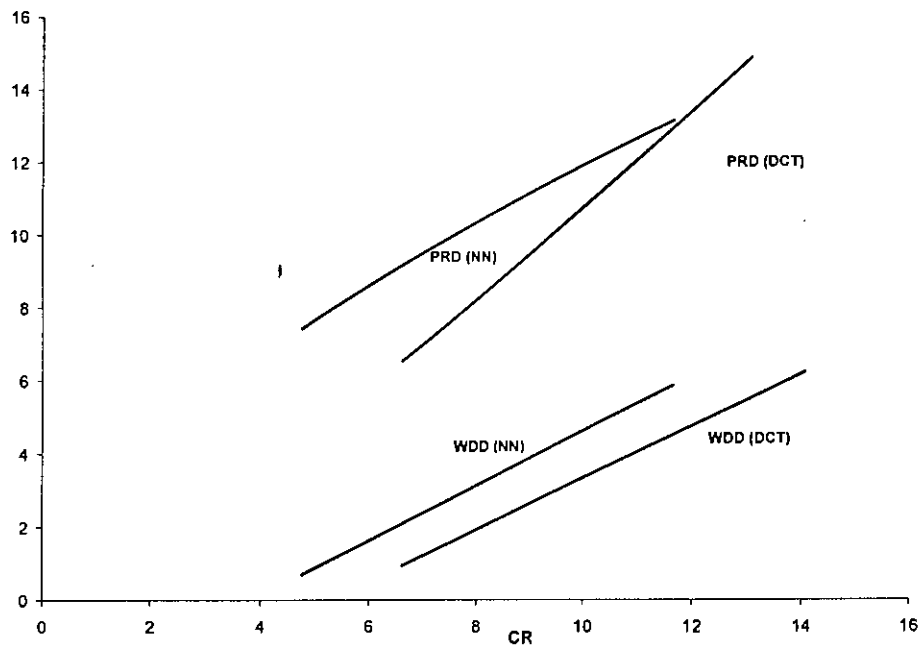


Figure 6.14: The distortion-rate curves of DCT-RLE and NN based schemes for MIT-BIH record 101

Chapter 7

CONCLUSION

7.1 Discussion

In this research, an algorithm for compressing ECG signals using 1-D DCT and RLE is described and experimental results from applying this method to different MIT-BIH database records are presented. The effects of different step size of quantization, bit rates, feature distortions and compression ratios are examined. The final choice of optimal threshold for quantization in ECG compression application depends on the reconstructed signal's quality along with the ability of clinical diagnosis. To facilitate the comparison of our proposed algorithm with other well known algorithms, we have also implemented a NN based compression scheme.

From our results we find that the 2-stage RLE with Huffman coding on quantized DCT coefficients performed better than NN based compression. Also, from the distortion rate curves, it can be concluded that the compressor performs worst if we decrease the bit rate lower than 200 bps for all the presented datasets. The result coincides both for the numerical and visual distortion measures through PRD and WDD indices respectively. Review by cardiologists suggest that with a compression ratio of 15:1, the memory requirement of the digital recording will be reduced to 2.85 Mbytes for a single lead system, 11-bit amplitude resolution with sampling rate 360 Hz. With the availability of low cost portable storage devices and digital signal processors, using the proposed methodology, it will be possible to overcome the limitation of bandwidth for real time data transfer in emergency medical situations. Here the main strength of this algorithm is the use of WDD based feature extraction instead of numerical analysis of the reconstructed ECG data.

7.2 Future Perspectives

In any compression system the target is to present the recovered signal as much as original one with lowest possible bit rate. Here, if we can apply fixed length window for segmentation of ECG, then it will be possible to introduce 2-D DCT on the time domain data. Then it will be possible to apply beat code book or long term prediction on that data. This will improve the performance of our system by increasing the CR with lower reconstruction error. This can be done before DCT conversion of the data to obtain the generalized pattern of each ECG beat. Our future work is aimed towards this improvisation. Here we have used only three records of MIT-BIH, because application of these three records was found in all most the researches. So this helps us to compare the results with others. Using a wide range of different database records can materialize our concept to reality. By using simple and efficient adaptive quantization strategy of the non-zero DCT coefficients, our compressor can improve its performance. A simple and effective binary lookup table can be formed by using beat code book that will improve considerably the storage efficiency and also less header wastage for Huffman dictionary.

The compression system may be more computationally complex than most of the published ECG compression algorithms. But, it can be possible to implement in real time using inexpensive DSP chips. From the point of view of computational complexity, the diagnostic feature extraction for WDD measure can be made faster by integrating it as a tool to the compressor. Complexity can also be reduced by the extraction of fewer features, or by developing more efficient extraction algorithms.

APPENDIX

Characteristics of ECG Test Signals from MIT-BIH

Record Number	Subject	Primary Rhythm and Morphology
100	Male, age 69	Normal sinus rhythm (NSR)
101	Female, age 75	Normal sinus rhythm (NSR), normal conduction
102	Female, age 84	Normal sinus rhythm, Paced rhythm
103	Male (age not recorded)	NSR, Atrial premature contraction (APC)
104	Female, age 66	NSR, Preventricular contractions (PVC)
105	Female, age 73	Normal sinus rhythm, high-grade noise and artifact
106	Female, age 24	NSR, noise in lower signal, Ventricular tachycardia
107	Male, age 63	Paced rhythm, complete heart block
108	Female, age 87	First degree AV block and sinus arrhythmia
109	Male, age 64	NSR, left bundle branch block
111	Female, age 47	NSR, left bundle branch block, first degree AV block
112	Male, age 54	APC, S-T segment depression in the upper channel
115	Female, age 39	NSR, Sinus arrhythmia, Baseline wander in lower signal
116	Male, age 68	NSR, Preventricular contractions (PVC)
117	Male, age 69	Normal sinus rhythm
118	Male, age 69	NSR, right bundle branch block
119	Female, age 51	Normal sinus rhythm, Ventricular trigeminy
121	Female, age 83	Normal sinus rhythm, Noise in lower signal
122	Male, age 51	NSR, low-amplitude high-frequency noise
123	Female, age 63	Sinus arrhythmia, Interpolated PVC
124	Male, age 77	Multiform PVCs, Accelerated junctional rhythm
200	Male, age 68	Atrial fibrillation, PVCs are uniform and late-cycle
202	Male, age 68	Normal sinus rhythm, PVCs
205	Male, age 59	Ventricular tachycardia, Noise in lower signal
207	Female, age 89	NSR, first degree AV block and left bundle branch block
209	Male, age 62	Atrial premature contraction (APC), PVCs
210	Male, age 89	Atrial fibrillation, Ventricular tachycardia
214	Male, age 53	NSR with left bundle branch block and PVC
228	Female, age 80	Ventricular bigeminy, First degree AV block
231	Female, age 72	2 ^o heart block, Blocked APC

REFERENCES

- [1] Manikandan, M. S., and Dandapat, S., "Wavelet-Threshold based ECG Compression with smooth retrieved quality for Telecardiology", *ICISIP 2006*, pp 138-143.
- [2] Mohammadpour, T. I., Mollaei, M. R. K., "ECG Compression with Thresholding of 2-D Wavelet Transform Coefficients and Run Length Coding", *Euro. J. Sci. Research*, vol-27, pp 248-257, 2009.
- [3] Cox, J. R, Nolle, F. M., Fozzard, H. A. and Oliver, G. C., "AZTEC, a preprocessing program for real time ECG rhythm analysis," *IEEE Trans. Biomed. Eng.*, vol-15, pp 128-129, 1968.
- [4] Mueller, W. C., "Arrhythmia detection program for an ambulatory ECG monitor." *Biomed. Sci. Instrument.*, vol-14, pp 81-85, 1978.
- [5] Jalaaladdin, S, Strattan, R and Coberly, W, "ECG data compression techniques-A unified approach," *IEEE Trans. Biomed. Eng.*, vol-37, pp 329-343, 1990.
- [6] Hilton, M., "Wavelet and wavelet packet compression of electrocardiograms", *IEEE Trans. Biomed. Eng.*, vol-44, pp 394-400, 1997.
- [7] Batista, L., Melcher, E. U. K., Carvalho, L. C, "Compression of ECG signals by optimized quantization of discrete cosine transform coefficients", *Med. Eng. & Physics*, vol-23, pp 127-134, 2001.
- [8] Benzid, R., Messaoudi, A. and Boussaad, A., "Constrained ECG compression algorithm using the block-based discrete cosine transform", *Dig. Sig. Proc.*, Elsevier, vol-18, pp 56-64, 2008.
- [9] Manikandan, M. S., Dandapat, S., "ECG distortion measures and their effectiveness", *Proc. Int. Conf. on Emerging Trends in Eng. And Tech.*, vol-00, pp 705-710, 2008.
- [10] Blanco-Velasco , M., Cruz-Rold'ana , F., Godino-Llorenteb , J. I., Blanco-Velasco, J., Armiens-Aparicioa, C. and L'opez-Ferrerasa, F. "On the use of

- PRD and CR parameters for ECG compression”, *J. Med. Eng. and Phy.*, vol-27, pp 798-802, 2005.
- [11] Zigel, Y., Cohen, A. and Katz, A., “The weighted diagnostic distortion (WDD) measure for ECG signal compression”, *IEEE Trans. Biomed. Eng.*, vol-47, 2000.
- [12] Zigel, Y., Cohen, A., Katz, A., “A diagnostic meaningful distortion measure for ECG compression,” *Proc. 19th Conf. IEEE.*, pp 117–120, 1996.
- [13] Zigel, Y., “ECG Signal Compression”, *M.Sc. Thesis*, Ben-Gurion University, Israel, 1998.
- [14] Huszar, R.J. “*Basic Dysrhythmias: interpretation & management*”, 2nd ed. St. Louis, Missouri: Mosby Lifeline, 1994.
- [15] Laguna, P., Thakor, N.V., Caminal, P., Jane, R., and Yoon, H-R. “New algorithm for QT interval analysis in 24-hour Holter ECG: performance and applications”, *J. on Med. and Biol. Eng. and Comp.*, vol-28, pp 67-73, 1990.
- [16] Tompkins, W.J., “*Biomedical Digital Signal Processing*”, Englewood Cliffs, New Jersey: Prentice-Hall, 1993.
- [17] Moody, G.B., Soroushian, K., and Mark, R.G., “ECG data compression for tapeless ambulatory monitors”, *J. on Comp. in Cardio.*, pp 467-470, 1988.
- [18] Cohen, A., Poluta, P.M., & Scott-Millar, R. “Compression of ECG signals using vector quantization”, *Proc. of the IEEE-90 S. A. Symp. Comm. and Sig. Proc.*, COMSIG-90, pp 45-54, 1990.
- [19] Khayam, S A, “The Discrete Cosine Transform (DCT): Theory and Application”, *ECE, Info. Theory and Coding*, pp 602-802, 2003.
- [20] Novák, D, “Processing of ECG signal using Wavelets”, *M. Sc. Thesis*, Czech Technical University, Prague, Czech Republic.
- [21] Lee H, Buckley K. “ECG data compression using cut and align beats approach and 2-D transforms”, *IEEE Trans. Biomed. Eng.*, vol-46, pp 64-556, 1999.
- [22] Ahmed N, Milne P, Harris S. “Electrocardiographic data compression via orthogonal transforms”, *IEEE Trans. Biomed. Eng.*, vol-22, pp 7-484, 1975.
- [23] Zou F, Gallagher R. “ECG data compression with wavelet and discrete cosine transforms”, *Biomed. Sci Instrum*, vol-30, pp 57–62, 1994.

- [24] D. Huffman, "A method for the construction of minimum redundancy codes," *Proc. of IRE*, vol-40, pp. 1098–1101, 1952.
- [26] Oh, S. "A new quality measure in Electrocardiogram Signal", *M. Sc. Thesis*, University of Florida, USA, 2004.
- [27] Hu, Y. H., Tompkins, W. J., Urrusti, J. L. and Afonso, V. X. "Applications Artificial Neural Netwrks for ECG signal detection and classification", *J. Elec. Cardio.*, vol-6, pp 66-73, 1993.
- [28] Neural Simulator (Version 2.0). <http://teacher.buet.ac.bd/sid>.
- [29] Zigel, Y., Cohen, A., Abu-Ful, A, Wagshal, A, Katz, A, "Analysis by Synthesis ECG Signal Compression", *Comp. Cardio.*, vol-24, pp 279–92, 1997.

